



**HAL**  
open science

## Source-to-sink dynamics in the Kyrgyz Tien Shan from the Jurassic to the Paleogene: Insights from sedimentological and detrital zircon U-Pb analyses

Elien de Pelsmaeker, Marc Jolivet, Amandine Laborde, Marc Poujol, Cécile Robin, Fedor I. Zhimulev, Simon Nachtergaele, Stijn Glorie, Shana de Clercq, Vladislav Yu Batalev, et al.

### ► To cite this version:

Elien de Pelsmaeker, Marc Jolivet, Amandine Laborde, Marc Poujol, Cécile Robin, et al.. Source-to-sink dynamics in the Kyrgyz Tien Shan from the Jurassic to the Paleogene: Insights from sedimentological and detrital zircon U-Pb analyses. *Gondwana Research*, 2018, 54, pp.180-204. 10.1016/j.gr.2017.09.004 . insu-01621293

**HAL Id: insu-01621293**

**<https://insu.hal.science/insu-01621293>**

Submitted on 23 Oct 2017

**HAL** is a multi-disciplinary open access archive for the deposit and dissemination of scientific research documents, whether they are published or not. The documents may come from teaching and research institutions in France or abroad, or from public or private research centers.

L'archive ouverte pluridisciplinaire **HAL**, est destinée au dépôt et à la diffusion de documents scientifiques de niveau recherche, publiés ou non, émanant des établissements d'enseignement et de recherche français ou étrangers, des laboratoires publics ou privés.

## Accepted Manuscript

Source-to-sink dynamics in the Kyrgyz Tien Shan from the Jurassic to the Paleogene: Insights from sedimentological and detrital zircon U-Pb analyses

Elien De Pelsmaecker, Marc Jolivet, Amandine Laborde, Marc Poujol, Cécile Robin, Fedor I. Zhimulev, Simon Nachtergaele, Stijn Glorie, Shana De Clercq, Vladislav Yu. Batalev, Johan De Grave



PII: S1342-937X(17)30067-9  
DOI: doi:[10.1016/j.gr.2017.09.004](https://doi.org/10.1016/j.gr.2017.09.004)  
Reference: GR 1863

To appear in:

Received date: 27 January 2017  
Revised date: 29 August 2017  
Accepted date: 14 September 2017

Please cite this article as: Elien De Pelsmaecker, Marc Jolivet, Amandine Laborde, Marc Poujol, Cécile Robin, Fedor I. Zhimulev, Simon Nachtergaele, Stijn Glorie, Shana De Clercq, Vladislav Yu. Batalev, Johan De Grave , Source-to-sink dynamics in the Kyrgyz Tien Shan from the Jurassic to the Paleogene: Insights from sedimentological and detrital zircon U-Pb analyses. The address for the corresponding author was captured as affiliation for all authors. Please check if appropriate. Gr(2017), doi:[10.1016/j.gr.2017.09.004](https://doi.org/10.1016/j.gr.2017.09.004)

This is a PDF file of an unedited manuscript that has been accepted for publication. As a service to our customers we are providing this early version of the manuscript. The manuscript will undergo copyediting, typesetting, and review of the resulting proof before it is published in its final form. Please note that during the production process errors may be discovered which could affect the content, and all legal disclaimers that apply to the journal pertain.

**Source-to-sink dynamics in the Kyrgyz Tien Shan from the Jurassic to the Paleogene:  
insights from sedimentological and detrital zircon U-Pb analyses.**

Elien De Pelsmaeker<sup>1,\*</sup>, Marc Jolivet<sup>2</sup>, Amandine Laborde<sup>3</sup>, Marc Poujol<sup>2</sup>, Cécile Robin<sup>2</sup>, Fedor  
I. Zhimulev<sup>4</sup>, Simon Nachtergaele<sup>1</sup>, Stijn Glorie<sup>5</sup>, Shana De Clercq<sup>1</sup>, Vladislav Yu. Batalev<sup>6,†</sup>,  
Johan De Grave<sup>1</sup>

<sup>1</sup>Department of Geology, Ghent University, Krijgslaan 281.S8, WE13, 9000 Gent, Belgium

<sup>2</sup>Université de Rennes 1, Laboratoire Géosciences Rennes, UMR 6118 CNRS/INSU, Campus  
de Beaulieu, 35042 Rennes, France

<sup>3</sup>Institut de Physique du Globe de Paris, Sorbonne Paris Cité, Université Paris Diderot, UMR  
7154 CNRS, Paris, France.

<sup>4</sup>Sobolev Institute of Geology and Mineralogy Siberian Branch Russian Academy of Sciences,  
Novosibirsk, Russia.

<sup>5</sup>Tectonics, Resources and Exploration (TraX), Department of Earth Sciences, University of  
Adelaide, Adelaide, Australia

<sup>6</sup>Research Station of the Russian Academy of Sciences, Bishkek, 720049, Kyrgyzstan

\*Corresponding author:

Department of Geology, Ghent University

Krijgslaan 281.S8, WE13, 9000 Gent, Belgium

Elien.DePelsmaeker@UGent.be

†In loving memory of Vlad Batalev, October 1955 – August 2017.

**Abstract**

New insights in the Mesozoic geodynamic evolution and related basin-range interactions in the Kyrgyz Tien Shan were obtained based on new sedimentological and detrital zircon U-Pb (LA-ICP-MS) results from Jurassic to Paleogene sedimentary sequences. Studied sedimentary sections are located in the Fergana and Yarkand-Fergana basins to the west of the Talas-Fergana Fault (TFF) and in the Issyk-Kul and Ming-Kush-Kökömeren basins to the east. The ages of the Phanerozoic zircon grains found in 18 Jurassic to Paleogene sandstones can be divided into four groups: Caledonian (470-390 Ma), Hercynian (315-260 Ma), Triassic (250-210 Ma) and Jurassic (190-160 Ma) ages. The differences in sedimentation pattern and zircon U-Pb results suggest that the TFF played an important role in the distribution of the sedimentary deposits in the Mesozoic. During the Early - Middle Jurassic, the TFF was active and the strongest subsidence occurred in the Yarkand-Fergana Basin. The provenance of its sediments can be explained both by local sources close to the TFF and by more distal sources to the (south)west, probably stretching into the present-day Pamir. During the Late Jurassic – Early Cretaceous, renewed compression led to the inversion of the Yarkand-Fergana Basin. Around the Jurassic – Cretaceous transition, large alluvial fans developing in a semi-arid to arid climate traceable around the whole Tien Shan were also deposited in the Fergana Basin. A mafic sill intruded within these alluvial fans provides an emplacement age of  $144 \pm 8$  Ma (apatite U-Pb) indicating (sub)volcanic activity during the Early Cretaceous. During the Late Cretaceous to early Paleogene, the area to the west of the TFF experienced marine incursions related to the proto-Paratethys Sea. The dominance of Caledonian ages in the Upper Cretaceous – lower Paleogene detrital samples indicates a change in provenance whereby the drainage areas became larger towards low-relief land area east of the TFF.

**Research highlights**

- Source-to-sink study in the Kyrgyz Tien Shan from the Jurassic to early Paleogene
- Detrital zircon U-Pb data from eighteen Jurassic to Paleogene sandstones
- Detailed sedimentary logging of key locations in the Kyrgyz Tien Shan basins
- Evidence for a major role of the Talas-Fergana Fault during the Mesozoic
- Change from humid to arid climate during Jurassic - Cretaceous transition

**Keywords**

Tian Shan; Talas-Fergana Fault; Central Asian Orogenic Belt; detrital zircon U-Pb dating; sedimentary logging; paleo-depositional environments

ACCEPTED MANUSCRIPT

## 1. Introduction

The Tien Shan currently represents an intracontinental mountain belt that extends from West to East through Uzbekistan, Kazakhstan, Tajikistan, Kyrgyzstan and China (Xinjiang province) over a distance of more than 2000 km. The Tien Shan forms the SW part of the Central Asian Orogenic Belt (CAOB), and is largely formed on Precambrian to Paleozoic basement (e.g. Windley et al., 2007; Xiao et al., 2015) (Fig. 1). The CAOB is characterized by multiple Paleozoic accretion-collision events, related to the closure of the Paleo-Asian Ocean and associated basins, leading to amalgamation of the Kazakhstan paleocontinent with the Siberia, Baltica, Tarim and North China cratons (e.g. Şengör et al., 1993; Windley et al., 2007; Wilhem et al., 2012; Liu et al., 2013, 2014; Xiao et al., 2013; Xiao and Santosh, 2014; Gillespie et al., 2017). Final amalgamation with associated deformation and magmatism took place during the Permian, followed by localized reactivation episodes during the Mesozoic and Cenozoic (e.g. Van der Voo et al., 2006; Burtman, 2015; Glorie and De Grave, 2016; Kaßner et al., 2016). These reactivation episodes are generally associated with far-field effects of several accretion-collision events along the (Eur)Asian margins whereby deformation is often partitioned along the inherited structural fabric of the ancestral orogen (e.g. Sengör, 1984; Watson et al., 1987; Dumitru et al., 2001; De Grave et al., 2007; Glorie et al., 2011; Macaulay et al., 2014; Jolivet, 2015). Subsequently, intracontinental orogens, such as Tien Shan, were built superimposed on the inherited basement architecture and the erosion products of their exhuming mountain ranges accumulated in sedimentary basins (Figs. 1; 2). In the Tien Shan, the currently active late Cenozoic compressional phase, driven by the convergence of the Indian and Eurasian plates, induces uplift and deformation (e.g. Molnar and Tapponnier, 1975).

In contrast to the well-studied pre-Mesozoic (e.g. Konopelko et al., 2007; 2008; 2009; 2012; 2014; 2017a,b; Windley et al., 2007; Alekseev et al., 2009; Glorie et al., 2010; De Grave et al., 2011; Seltmann et al., 2011; Kröner et al., 2012; 2013; Biske et al., 2013; Alexeiev et al., 2015, 2016) and Cenozoic (e.g. Sobel and Dumitru, 1997; Burbank et al., 1999; Abdrakhmatov et al., 2001; Bullen et al., 2001; 2003; Glorie et al., 2011; Goode et al., 2014; Macaulay et al., 2014; Bande et al., 2015a) history of the Kyrgyz Tien Shan, its Mesozoic geodynamic evolution remains less understood. This study presents new sedimentological information and detrital zircon U-Pb data on Mesozoic - early Cenozoic sedimentary units in the Issyk-Kul, Ming-Kush-Kökömeren, Fergana and Yarkand-Fergana basins (following the nomenclature of Allen et al., 2001; Bachmanov et al., 2008 and De Grave et al., 2011; Fig. 2) chiefly in order to shed light on the source-to-sink dynamics and paleotopographic evolution of the Kyrgyz Tien Shan from the Jurassic to the Paleogene. In addition, our results provide new insights into the Mesozoic geodynamic evolution and related basin-range interactions in the Kyrgyz Tien Shan.

## **2. Geological setting**

### **2.1 Pre-Mesozoic basement architecture**

Paleozoic complexes in the Kyrgyz Tien Shan are traditionally divided into three major tectonic units: Northern Tien Shan (NTS), Middle Tien Shan (MTS) and Southern Tien Shan (STS) (e.g. Windley et al., 2007; Konopelko et al., 2008; Glorie et al., 2010, 2011; Seltmann et al., 2011; De Grave et al., 2012; 2013; Biske et al., 2013; Alexeiev et al., 2016) (Fig. 2).

The NTS mainly consists of Precambrian continental fragments intruded by large volumes of Cambrian to Silurian granitoids with a peak igneous activity between 450 and 435 Ma (Late Ordovician to early Silurian) related to major subduction and collision events accompanying the formation of the Kazakhstan paleocontinent (Glorie et al., 2010; Kröner et al., 2012, 2013; Alexeiev et al., 2016). The NTS is additionally affected by Late Devonian - Carboniferous magmatism associated with the evolution of the Yili continental arc, and by Early Permian post-collisional granitoids (Konopelko et al., 2008; Biske and Seltmann, 2010; Degtyarev, 2011; Kröner et al., 2013). The NTS is now separated from the MTS by the EW oriented Nikolaev Line, which represents a combination of late Paleozoic thrusts and strike-slip faults (Fig. 2). To some extent it runs subparallel to, but does not coincide with, the Ordovician Terskey suture (e.g. Burtman, 2010). The NTS and MTS units were welded together during the Middle Ordovician (ca 460 Ma) and subsequently evolved as the southern margin of the Kazakhstan paleocontinent from the Silurian up to the Pennsylvanian (Alexeiev et al., 2016). The MTS consists of a Precambrian microcontinent in the north and an Ordovician arc in the south (e.g. Alexeiev et al., 2016; Kröner et al., 2017). The microcontinent consists of Paleoproterozoic gneisses, Neoproterozoic granitoids and felsic volcanic rocks, overlain by Neoproterozoic to Ordovician passive margin sediments (Alexeiev et al., 2016; Kröner et al., 2017). The arc in the south, within the present-day Chatkal, Bozbutau, and Atbashi ranges, consists of Middle to Late Ordovician intermediate and felsic volcanic rocks. In the southwestern Kurama, Chatkal and Atbashi ranges, this collage is affected by Silurian - Early Devonian (ca 435 to 410 Ma) and late Mississippian - Pennsylvanian (ca 325-310 Ma) arc magmatism (Biske and Seltmann, 2010; Seltmann et al., 2011; Burtman, 2015; Alexeiev et al., 2016; Dolgoplova et al., 2017; Konopelko et al., 2017b; Fig. 2). In addition, Permian (ca 295-270 Ma) collisional and post-collisional magmatic

rocks, related to the closure of the late Paleozoic Turkestan Ocean, were emplaced in the MTS (Konopelko et al., 2007; Biske and Seltmann, 2010; De Grave et al., 2011; 2013; Seltmann et al., 2011; Konopelko et al., 2017b; Fig. 2). In central Kyrgyzstan, the MTS and STS are separated by the ophiolite-bearing Atbashi-Inylchek or South Tien Shan suture which formed around 310-280 Ma (e.g. Konopelko et al., 2007; Loury et al., 2016).

In contrast to the NTS and MTS, which are dominated by Precambrian crustal fragments and were amalgamated to the Kazakhstan paleocontinent during the early and middle Paleozoic, the STS represents a late Paleozoic accretionary complex and collisional belt related to the Pennsylvanian closure of the Turkestan Ocean (ca 300 Ma) and subsequent collision of the Kazakhstan paleocontinent (including the NTS and MTS) to the north, with the Tarim and Afghan-Tajik microcontinents to the south (e.g. Windley et al., 2007; Alekseev et al., 2009; Biske and Seltmann, 2010; Biske et al., 2013; Burtman, 2015; Alexeiev et al., 2016; Käßner et al., 2016; Loury et al., 2016). The STS consists of Silurian to Lower Permian trench and passive margin sediments and igneous rocks (Konopelko et al., 2007; Kröner et al., 2008; Alekseev et al., 2009; Biske and Seltmann, 2010; Glorie et al., 2011; Seltmann et al., 2011; Alexeiev et al., 2015; Loury et al., 2016; Dolgoplova et al., 2017). The closure of the Turkestan ocean led to the final assembly of the ancestral Tien Shan during the Pennsylvanian – Permian and was accompanied by significant collisional and post-collisional magmatism, peaking between 300 and 270 Ma. Subsequently, the entire Tien Shan experienced transpressive deformation during the Permian – Early Triassic, which was responsible for dispersed rotations and shear movements along strike-slip faults (e.g. Bazhenov et al., 1999; Van der Voo et al., 2006; Rolland et al., 2013; Burtman, 2015). One of the most prominent faults is the NW-SE oriented Talas-Fergana Fault (TFF), that intersects the NTS, MTS and STS (Fig. 2). The TFF played an important role in the post-Paleozoic

evolution of the Tien Shan (Burtman et al., 1996; Allen et al., 2001; Konopelko et al., 2013; Rolland et al., 2013; Alexeiev, et al., 2017).

## 2.2 Mesozoic and Cenozoic evolution

Since the Mesozoic, the area has been repeatedly reactivated in an intracontinental setting as a consequence of distant collision-accretion events (e.g. Sengör, 1984; Watson et al., 1987; Hendrix et al., 1992; De Grave et al., 2007; Jolivet et al., 2010; Macaulay et al., 2014). The extent of these reactivations and their direct link with specific events at the plate's margin is still a matter of ongoing research (e.g. Sobel et al., 2006a; De Grave et al., 2007; Jolivet et al., 2013b; Macaulay et al., 2014; Bande et al., 2015b; Yang et al., 2015; Glorie and De Grave, 2016). Along the southern Eurasian margin, several Mesozoic accretion-collision events (grouped as the Cimmerian Orogeny) took place, inducing reactivation and deformation in the Tien Shan (e.g. Sengör, 1984; Watson et al., 1987; Yin and Harrison, 2000; Dumitru et al., 2001; Angiolini et al., 2013; De Grave et al., 2013; Yang et al., 2013; Jolivet, 2015). These events include the collision of the Qiangtang block during the Late Triassic - Early Jurassic, the Lhasa block during the Late Jurassic - Early Cretaceous and the Kohistan-Ladakh arc during the Late Cretaceous (e.g. Yin and Harrison, 2000; Roger et al., 2010; Jolivet, 2015). In addition, the Jurassic – Cretaceous geodynamic evolution of Central Asia was marked by the diachronous closure of the Mongol-Okhotsk Ocean, connecting Mongolia – North China to Siberia (Zorin, 1999; Metelkin et al., 2010; Wilhem et al., 2012 and references therein). However, both the tectonic and topographic implications of this event are still debated and it seems that this event mainly affected the areas to the northeast of the Tien Shan (e.g. the Altai-Sayan region; De Grave et al., 2008; 2009; Glorie et al., 2012; Jolivet et al., 2013a; Glorie and De Grave, 2016; Jolivet et al., 2017).

In the Cenozoic, the main compressive deformation phase leading to basement exhumation in the Tien Shan initiated during the late Oligocene – Miocene and is related to the ongoing India-Eurasia convergence (e.g. Molnar and Tapponnier, 1975; Tapponnier and Molnar, 1979; Abdrakhmatov et al., 1996; 2001; Sobel, 1999; Thomas et al., 1999; Bullen et al., 2001; Coutand et al., 2002; Charreau et al., 2006; Sobel et al., 2006a; De Grave et al., 2007; 2012; Heermance et al., 2008; Yin, 2010; Macaulay et al., 2014; Yang et al., 2015).

### **2.2.1 Talas-Fergana Fault and associated Yarkand-Fergana Basin**

The intracontinental right-lateral strike-slip Talas-Fergana Fault (TFF) represents the southern part of the larger Karatau – Talas – Fergana Fault that extends for 1500 km from southern Turgai in Kazakhstan to western Tarim in China (Burtman, 1964; 2015; Burtman et al., 1996; Sobel, 1999; Allen et al., 2001; Konopelko et al., 2013; Rolland et al., 2013; Bande et al., 2015b; Alexeiev et al., 2017) (Fig. 2). The crosscutting relationships of the TFF with early and middle Permian structural elements of the STS indicate that the TFF formed, as a strike-slip fault, no earlier than the middle Permian (Burtman et al., 1996; Lomize, 1996; Bazhenov et al., 1999; Alexeiev et al., 2017). As summarized by Alexeiev et al. (2017), the strike-slip kinematics along the TFF evolved during three stages in (1) the late Permian and Triassic (with estimated maximum offset up to 70 km), (2) the Early and Middle Jurassic (with estimated maximum offset up to 70 km), and (3) the late Cenozoic (with estimated maximum offset up to 60 km). These offset values refer to the maximum estimates from within the Fergana Range. They decrease along the strike of the fault both to the north and south. Konopelko et al. (2013) and Rolland et al. (2013) constrained the timing of the first-stage deformation from late Permian to Middle Triassic (256-240 Ma) by  $^{40}\text{Ar}/^{39}\text{Ar}$

dating of syn-kinematic micas from the fault zone. The second-stage strike-slip deformation occurred during the Early and Middle Jurassic, and is related to the formation of the northwest-southeast striking Aryskum (in South Turgai), Leontiev (or Leontievka) and Yarkand-Fergana grabens, which represent fault-bend and pull-apart basins (e.g. Burtman et al., 1996; Lomize, 1996; Sobel, 1999; Allen et al., 2001; Yin et al., 2012; Alexeiev et al., 2017) (Fig. 2). The South Turgai Basin is characterized by an imbricate fan of normal and normal-strike-slip splays, making up a horsetail structure (Allen et al., 2001; Yin et al., 2012; Alexeiev et al., 2017). It locally contains up to 4500m of non-marine clastic Jurassic sediments. In the Leontiev Graben, the Jurassic sedimentary succession can reach up to ca 2 km (Buvalkin et al., 1991; Sobel, 1999; Schnyder et al., 2016). The Yarkand-Fergana Basin is a transtensional pull-apart basin located along the western side of the TFF in southern Kyrgyzstan and extends southwards into the western Tarim (Burtman et al., 1996; Sobel, 1999; Allen et al., 2001; Alexeiev et al., 2017) (Fig. 2). This Meso-Cenozoic basin presents a remarkably thick (> 5km) succession of Jurassic sediments in close vicinity to the fault (Belgovskiy et al., 1958; Shlezinger, 1971). The sedimentary thickness decreases away from the fault and the sediments are intensively faulted and folded (Belgovskiy et al., 1958; Shlezinger, 1971). The third strike-slip deformation stage along the TFF developed from the late Oligocene (ca 25 Ma) until the present day (e.g. Burtman et al., 1996; Bande et al., 2015b; Alexeiev et al., 2017). Several studies (e.g. Burtman, 2012; Korzhenkov et al., 2014; Feld et al., 2015; Tibaldi et al., 2015) pointed out that the TFF is still active, with an average slip rate estimated at ~9-14 mm/a based on radiocarbon dating of terraces displaced by the fault (Burtman et al., 1996; Trifonov et al., 2015).

Published information concerning the sedimentary successions in the Kyrgyz part of the Yarkand-Fergana Basin is scarce in English literature, however, Sobel (1999)

studied the Mesozoic deposits within the southern reaches of the basin in China and Yang et al. (2014) provided the first source-to-sink study in the same region. Sobel (1999) showed that the Lower Jurassic strata rest unconformably on Precambrian-Paleozoic basement rocks and that the sedimentary deposition was controlled by numerous faults. The Lower Jurassic series consist of conglomerates, sandstones, siltstones and mudstones with plant fossils and coal layers. They were interpreted by Sobel (1999) as alluvial fan, fluvial and lacustrine or swamp facies, deposited in a humid environment. The lower Middle Jurassic in that part of the basin consists of fluvial conglomerates on the eastern margin of the basin, whereas the western region was dominated by lacustrine and swamp deposits. The upper Middle Jurassic strata represent shallow lacustrine, fluvial and floodplain deposits. The Upper Jurassic – Lower Cretaceous transition is characterized by a 400m thick conglomeratic fluvial-channel complex whereas the Lower Cretaceous deposits are characterized by fluvial red beds and the Cenomanian-Turonian by lagoon deposits. During the Late Cretaceous and early Paleogene, a shallow marine depositional environment was established, where an epicontinental sea connected the Yarkand-Fergana, Fergana, SW-Tarim and Tajik basins (e.g. Dercourt et al., 1993; Cobbold et al., 1994; Sobel, 1999; Bosboom et al., 2011).

### **2.2.2 Fergana Basin**

The Meso-Cenozoic intramontane Fergana Basin is located to the west of the TFF and extends from Kyrgyzstan into Uzbekistan (Figs. 1; 2). The eastern part of the basin is surrounded by the Chatkal mountain range to the north, the Fergana range to the east and the Alai range to the south (Fig. 2). Mesozoic sediments, generally characterized by slow accumulation rates, crop out sporadically in the surrounding foothills and are also present in the subsurface of the basin (Kuzichkina, 1972; Aliev et al., 1981; Bande et al., 2015a).

Following the late Paleozoic assembly, building of the ancestral Tien Shan and deposition of Permian molasses, the region underwent erosion during the Triassic, leading to the formation of a regional peneplanation surface (Osmonbetov et al., 1982; Clarke, 1984; Bande et al., 2015a). Renewed subsidence started from the Early Jurassic and led to the accumulation of alluvial-plain, deltaic and lacustrine sediments. Lower and Middle Jurassic conglomerates, sandstones and coal-bearing shales, with a continental origin, unconformably overlie Paleozoic basement rocks (Osmonbetov et al., 1982; Cobbold et al., 1994). Upper Jurassic sediments are mainly represented by red beds of sandstones, siltstones, mudstones and conglomerates in which coal is mostly absent and plant remains are scarce (Osmonbetov et al., 1982; Clarke, 1984; Jolivet et al., 2015). Lower Cretaceous deposits vary from conglomerates, sandstones, mudstones, to limestones and evaporites (Cobbold et al., 1994; Burtman et al., 1996). During the Albian and Late Cretaceous, marine incursions related to a proto-Paratethys branch occurred in the Fergana Basin, as well as in the Tarim, Tajik and Alai basins (Dercourt et al., 1993; Cobbold et al., 1994; Burtman et al., 1996; Bande et al., 2015a). The calm tectonic environment persisted during the Paleocene-Eocene, with the deposition of circa 300m of low-energy, alluvial plain and lacustrine clastic sediments with alternations of marine strata (Bosboom et al., 2011; 2015; Bande et al., 2015a).

### **2.2.3 Issyk-Kul Basin and Ming-Kush-Kökömeren Basin**

Isolated outcrops of continental Jurassic and early Paleogene sediments (maximum a few hundred m thick) occur in the southern Issyk-Kul Basin (e.g. Kuzichkina, 1972; Cobbold et al., 1994; Macaulay et al., 2014) and west of lake Song Kul in the Ming-

Kush-Kökömeren Basin (Bebeshev, 1995; Bachmanov et al., 2008; Morozov et al., 2014) (Fig. 2).

In the Issyk-Kul Basin, Jurassic sediments mainly consist of sandstones and coal-bearing shales resting unconformably on Paleozoic basement (Kuzichkina, 1972; Osmonbetov et al., 1982; Cobbold et al., 1994). The Jurassic sediments are overlain by the thin Paleocene to early Oligocene Chonkurchak or Kokturpak Formation (Fm) which consists of continental red beds and lacustrine sediments (up to 100m thick) intercalated with some basaltic rocks (Turdukulov, 1987; Osmonbetov et al., 1982; Cobbold et al., 1994; Sobel and Arnaud, 2000; Wack et al., 2014). This formation is followed by the Oligocene-Miocene coarse-grained Kyrgyz and Shamsi formations (up to 2km thick) and alluvial-lacustrine Pliocene Issyk-Kul or Chu Fm (up to 3km thick) (Turdukulov, 1987; Macaulay et al., 2014; Wack et al., 2014).

The Ming-Kush-Kökömeren Basin is a narrow transpressive depression. The Jurassic sediments consist of sandstones, siltstones, coal-bearing shales and coal seams and rest unconformably on Carboniferous rocks. The thickness of the strata varies from 100m to 680m. The plant remains found in the coal deposits are largely typical for the Lower Jurassic, although some of them can occur in the Middle Jurassic as well (Lasovskiy and Mozolev, 1961; Bachmanov et al., 2008). The Jurassic series here are followed by the ca 40m thick Paleogene Kokturpak Fm and a local equivalent of the Kyrgyz Fm, i.e. the 'Ming-Kush conglomerates' which forms a thick package up to 800m (Lasovskiy and Mozolev, 1961; Bachmanov et al., 2008).

### **3. Samples, Methodology and Results**

### 3.1 Sampling sites

In this study we present new sedimentological and detrital zircon U-Pb data on Jurassic to Paleogene sedimentary units from the Fergana and Yarkand-Fergana basins to the west of the TFF and from the Issyk-Kul and Ming-Kush-Kökömeren basins to the east. Sedimentological characteristics of the Mesozoic sediments were obtained from detailed field logging of multiple, continuous sections (Figs. 2; 3; 4; 5). In the Fergana Basin, the two well-exposed Tash-Komyr and Jetim-Dobo sections include Jurassic, Cretaceous and early Paleogene series (Figs. 2; 3). In the southern part of the Yarkand-Fergana Basin, the Terek section includes Jurassic and Cretaceous series (Figs. 2; 4). Additional Jurassic-Cretaceous outcrops along the Chitty and Yassy rivers were studied and sampled in order to propose a broader geographic coverage (Fig. 2). In the Issyk-Kul Basin, Jurassic and early Paleogene sediments were studied near the villages of Kadji-Sai and Jeti-Oguz (Figs. 2; 5). In the Ming-Kush-Kökömeren Basin, the Ming-Kush section includes Jurassic, Paleogene and Neogene sediments (Figs. 2; 5). 18 samples, ranging from fine-, medium- to coarse-grained sandstones, were collected along these sections for detrital zircon U-Pb dating (Figs. 2; 3; 4; 5; Table 1).

### 3.2 Sedimentological analysis and interpretation

A general description of the sediment series exposed in the various sections is presented below and a more detailed description, with the addition of some field pictures, is provided as Supplementary Data A. A description of the main sedimentary features associated with the facies and their interpretation in terms of deposition environments are given in Table 2.

### 3.2.1 Fergana Basin

#### *Tash-Komyr section*

The Tash-Komyr section is located at the northeastern edge of the Fergana Basin, close to the town of Tash-Komyr (Fig. 2). The section was logged along two river incisions, one covering the Jurassic and one covering the Cretaceous and lower Paleogene with a total thickness of ~1450m (Fig. 3). The two parts of the section overlap and outcrop quality was excellent. The Paleogene section is recently briefly described and dated using magnetostratigraphy by Bosboom et al. (2015).

The Jurassic series rest unconformably on Pennsylvanian green-grey siltstones. The lowest ca 100 m of sediments represent Hjulström-type fan delta (LE1), shallow lake (LE2) and distal alluvial plain (AP2) deposits. They represent the Lower - Middle Jurassic (Toarcian - Aalenian; 183-174 Ma) Tash-Komyr Fm (Kuzichkina, 1972; Aliev et al., 1981). The next ca 100 m are interpreted as representing a distal alluvial plain environment (AP2) and belong to the Aalenian to Bathonian Igrysay Fm (Aliev et al., 1981; Kuzichkina, 1972). Oxidized layers interpreted as humid paleosols and numerous coal beds suggest a humid climate setting. The next ca 100 m correspond to shallow lake deposits (LE2; Supplementary Data A, Fig. a) and is followed by about 100 m of very distal, semi-arid alluvial plain deposits (AP2a) corresponding to the Bathonian to lower Oxfordian Balabansay Fm (Kuzichkina, 1972; Aliev et al., 1981). Root traces, calcareous nodules and some centimeter-thick calcareous paleosols indicate a semi-arid climate.

The Upper Jurassic - Cretaceous boundary is characterized by a remarkably thick (ca 110 m) massive clast-supported conglomerate unit with a strongly erosive base, i. e. the Hodzhiabad Fm (Poyarkova, 1972) (Supplementary Data A, Fig. c). Evidence of subaerial flash-flood to sheet-flood deposits indicates a proximal alluvial fan system (AF1). The proportion of sandstone increases towards the top of the unit, which is interpreted as a more distal alluvial fan (AF2). Carbonate impregnation of some of the upper layers may indicate the development of calcrete in a semi-arid climate although diagenetic, post-depositional fluid circulation cannot be excluded. This well-developed alluvial fan system forms the stratigraphic equivalent of the hyper-arid Kalaza Fm exposed in the northern and southern piedmonts of the Chinese Tien Shan (Fang et al., 2015; Jolivet et al., 2015). A mafic sill intruded in the Hodzhiabad conglomerates yields an apatite U-Pb age of ca 140 Ma (§ 3.3). The presence of (sub)volcanic rocks along the Naryn river near Tash Komyr was previously described by Verzilin (1976) and Rasskazov et al. (2015), who suggested an Early Cretaceous age based on their stratigraphic position. Based on the age obtained in this study and the Bathonian to early Oxfordian age suggested for the Balabansay Fm (Belgovskiy et al., 1958; Kuzichkina, 1972; Aliev et al, 1981) the age for the Hodzhiabad Fm is constrained to the Oxfordian to Valanginian.

The Hodzhiabad Fm is followed by a ca 50 m thick unit similar to the very distal, semi-arid alluvial plain (AP2a) deposits of the Balabansay Fm. It is followed by a ca 100 m thick sandier unit interpreted as a semi-arid Hjulström-type fan delta deposit (LE1; Supplementary Data A, Fig. d). Paleocurrents are mostly E-SE directed in the Lower Cretaceous series, which is very different from the generally W-directed paleocurrents in the Upper Jurassic sediments below. The following ca 250 m of the section contain numerous, decimeter- to meter-thick caliches and calcretes (Supplementary Data A, Fig. e-f). Several

dinosaur nests containing well-preserved eggs have been discovered within the upper part of the unit (Supplementary Data A, Fig. g). Although detailed analysis is still underway, the eggs are attributed to herbivorous Hadrosauridae dinosaurs of Coniacian to Maastrichtian age. The unit is interpreted as a semi-arid distal alluvial to lacustrine coastal plain (AP2a), probably with temporary lakes (LE2).

The uppermost Cretaceous – lower Paleogene series (ca 375 m) still contain numerous meter- to several-meter-thick caliche and calcrete layers. This unit is interpreted as a more proximal semi-arid alluvial plain deposit, without preservation of lake or swamp deposits (AP1a). The large thickness of the calcareous paleosols suggests an overall very slow sedimentation rate, allowing for long-lasting periods of soil formation.

The uppermost Cretaceous – lower Paleogene alluvial plain deposits are capped by a ca 100 m thick marine unit containing centimeter-thick oysters (Supplementary Data A, Fig. h) such as the Ypresian *Flemingostrea hemiglobosa* (Romanovskiy, 1880; Burtman, 2000) near the base and the Bartonian *Sokolowia buhsii* (Grewingk, 1853) near the top, both associated to the Suzak Fm (Vialov, 1948) and deposited in a protected embayment, varying from intertidal to subtidal conditions (MPE). These deposits would correspond to the third transgression of the proto-Paratethys sea in Central Asia (Bosboom et al., 2015). Finally, the top of the logged section is interpreted as a semi-arid distal alluvial plain deposit (AP2a).

### ***Jetim-Dobo section***

The Jetim-Dobo section is located south of the Jetim Dobo village, on the southeastern edge of the Fergana Basin (Fig. 2). The base of the exposed Jurassic outcrops

contains numerous plant remains and coal seams with silicified tree trunks, and are interpreted as deposited in a humid alluvial plain environment. Towards the top, swamp to shallow lake sediments contain fresh water bivalves and gastropod shells. Finally, within the uppermost part, several calcareous paleosols suggest a semi-arid climate.

The logged section was recorded along a cliff and covers the Cretaceous and lower Paleogene with generally good outcrop quality (Fig. 3). From the geological map (Biske and Zubtsov, 1985) the base of the logged section represents the Jurassic to Cretaceous transition. The first unit, ca 10 m thick, is interpreted as a distal alluvial fan deposit (AF2). The following ca 75 m thick unit is more distal and corresponds to a distal alluvial plain deposit (AP2). It is followed by a ca 175 m thick unit of shallow lake deposits subjected to a semi-arid climate (LE2) as indicated by calcareous paleosol layers. The next ca 200 m thick unit likely corresponds to a Hjulström-type fan delta with evidence of semi-arid climate near the base (LE1). The following ca 125 m unit is interpreted, by comparison to the third unit, as shallow lake deposits (LE2). Exposures are then lacking over a ca 250 to 300 m gap in which only a few coarse-grained deposits, visible near the top, might indicate distal alluvial plain (AP2) or Hjulström-type fan delta (LE1) deposits. The following ca 225 m thick unit is composed of two sub-units separated by a possible erosional unconformity overlain by a conglomerate showing mud clasts at the base and root traces near the top. Based on the geological map (Biske and Zubtsov, 1985), the second subunit corresponds to the Cretaceous – Paleogene transition. Decimeter-thick paleosols formed by caliches indicate semi-arid climate conditions. The whole unit is interpreted as deposited in a Hjulström-type fan delta (LE1), with the upper subunit being more proximal than the basal one.

The following Paleogene unit is ca 75 m thick and contains a typical proto-Paratethys sequence (Bosboom et al., 2014) with numerous marine bivalves and gastropods shells, including oysters. Like in the Tash-Komyr section, this unit is interpreted as deposited in a marine protected embayment varying from intertidal to subtidal conditions (MPE). The next ca 100 m thick unit represents very distal semi-arid alluvial plain deposits (AP2a). The unit is characterized by a massive ca 5 m thick paleosol formed by caliches, indicating a long period of extremely slow sedimentation rates in semi-arid conditions. Finally, the last few meters of the section are marked by a new episode of a proto-Paratethys transgression. The unit contains marine (oyster-dominated) shells, sometimes associated with strong bioturbation (horizontal burrows), and is deposited in a marine protected embayment varying from intertidal to subtidal conditions (MPE).

### **3.2.2 Yarkand-Fergana Basin**

#### ***Terek section***

Based on the geological map (Belgovskiy et al., 1958) and on Genkina (1977), the ca 2700m thick Terek section (Figs. 2; 4) covers the Middle Jurassic Chartaash Fm and a large part of the Cretaceous. Thrust faults and folds affect the base of the Jurassic section but the stratigraphic continuity of the series is preserved.

The base of the Jurassic series rests unconformably on Carboniferous metasediments. The first ca 25 m thick unit corresponds to a distal alluvial fan (AF2) probably evolving towards a proximal alluvial plain (AP1) near the top. It is followed by a ca 75 m thick unit of Hjulström-type fan delta deposits (LE1), evolving towards a more proximal

environment near the top. The next 450 m are composed of organic-rich, bioturbated flood deposits in a shallow lake environment (LE2) evolving towards a more proximal environment with increased fluvial input (LE1). The following 450 m of the section are poorly exposed, but seems very similar to the sediment facies observed in the previous unit and are interpreted therefore as deposited in a shallow lake environment (LE2). The next ca 250 m thick unit is interpreted as a shallow lake most distal deposit (LE3).

According to the geological map of Belgovskiy et al. (1958), the next ca 200 m of the section mark the transition between the Jurassic and the Cretaceous, although no absolute age or biostratigraphic data are available. The transition unit is much coarser than the underlying distal lake deposits and corresponds to a proximal alluvial fan environment (AF1; Supplementary Data A, Fig. b). The Jurassic – Cretaceous transition in Terek is very similar to that in Tash-Komyr (§ 3.2.1) and to many other sections in the piedmonts of the Tien Shan (Fang et al., 2015; Jolivet et al., 2015), some of them showing an angular unconformity at the base of the transition unit (e.g. Eberth et al., 2001; Jolivet et al., 2015). Although no angular unconformity was observed between the alluvial fan deposits and the underlying lake sediments, it might be probable that the base of the alluvial fan forms an unconformable surface and that some of the Jurassic series is missing. Based on discontinuous outcrops, the following ca 1300 m thick unit is interpreted as deposited in a shallow lake environment with rare emersion (LE2). The ca. 900 m thick upper exposed part of the section initiates with a gravel conglomerate marking a possible erosion surface. The sediments are interpreted as deposited in a distal alluvial plain environment with large river systems and probably few intermittent shallow lakes or swamps (AP2 with few LE2). No climate indicators have been observed but the complete absence of plant remains or even of organic matter advocates for a dry climate. The transition between the Cretaceous and

Paleogene and the Paleogene sediments have not been logged in detail. The Paleogene sediments are represented by gypsum, mudstones, siltstones and massive limestone layers sometimes with oysters; indicating a lagoon - shallow marine environment.

### 3.2.3 Issyk-Kul Basin and Ming-Kush-Kökömeren Basin

#### *Jeti-Oguz section*

The Jeti-Oguz section, southwest of Karakol city in the Issyk-Kul Basin (Fig. 2), is limited to a 12 m thick outcrop of Jurassic – lower Paleogene sediments (Fig. 5). The Jurassic series are unconformably deposited on lower Paleozoic granites and Carboniferous sandstones. The first 2 meters are strongly oxidized suggesting humid climate conditions. Although poorly documented, this unit is interpreted as a distal alluvial plain deposit (AP2). The following 10 meters are coarse-grained sediments with oxidized crusts and one calcareous paleosol at the top, indicating a switch towards semi-arid climate. This unit is interpreted as a semi-arid proximal alluvial plain deposit (AP1a). The final meter of the Jurassic outcrop is capped by a decimeter-thick calcrete indicating a paleosol and possibly corresponds to a semi-arid distal alluvial plain (AP2a) or to a Hjulström-type fan delta (LE1). Following a roughly 2 m gap in the outcrop, a meter-thick calcrete layer can be attributed to the Paleogene (Kuzichkina, 1972).

#### *Kadji-Sai section*

The Kadji-Sai section is located along the southern shore of lake Issyk-Kul (Fig. 2). The well-exposed Jurassic section is about 250 m thick and is unconformably covered by Paleogene sediments (Fig. 5).

The Jurassic series rest unconformably on lower Paleozoic granites. The contact is marked by a tectonic breccia related to a major Cenozoic fault that controls the uplift of the Terskey Range immediately to the south (De Grave et al., 2013; Macaulay et al., 2014). However, this fault does not seem to affect the Mesozoic series significantly. The base of the Jurassic series is composed of ca 25 m of coarse-grained sediments containing caliche-type paleosols indicative of a semi-arid climate. This unit is interpreted as a semi-arid distal alluvial fan deposit (AF2a). Stacked coarse-grained sediments displaying bioturbation as well as a combination of oxidized and calcareous layers form the following ca 120 m thick unit. It represents a proximal alluvial plain deposit (AP1), possibly with semi-arid depositional conditions at the base (AP1a). The next unit, ca 25 m thick, is more fine-grained. Near the top, oxidized layers with numerous plant fragments represent paleosols developed in warm and humid conditions. A centimeter-thick layer of calcite beef is observed a few meters above the base of the unit. This unit is interpreted as deposited in a shallow lake environment in a humid climate (LE2). The following 50 m thick unit is interpreted as a Hjulström-type fan delta deposit (LE1). The upper part of the Jurassic sequence is represented by a ca 50 m thick unit of red to yellow fine-grained sediment, interpreted as deposited in a most distal shallow lake with limited, distal fluvial input (LE3). The strong oxidation that affects the most fine-grained layers might represent diagenesis in organic-rich layers. According to Kuzichkina (1972), the Jurassic is unconformably covered by Paleogene sediments. No obvious unconformity can be seen in the field. The supposed Paleogene series

initiates with several yellow to pink, meter-thick calcretes developed in fine-grained sandstone layers interbedded with siltstones.

### ***Ming-Kush section***

The ca 650m thick Ming-Kush section is situated in the small Ming-Kush-Kökömeren Basin (Figs. 2; 5) and includes the Jurassic, Paleogene and Neogene series (stratigraphic ages based on Lasovskiy and Mozolev, 1961). Although the base of the series is not documented in our section, the Jurassic series rest unconformably on Mississippian red sandstones on the southern edge of the basin, whereas on the northern edge the Jurassic series show fault contacts with the metamorphic basement and lower Paleozoic granites (Lasovskiy and Mozolev, 1961).

The first ca 125 m thick unit of the logged section is largely fine-grained and contains several coal seams and a lot of plant fragments. Some oxidized layers suggest the occurrence of paleosols developed in a humid climate. This unit is interpreted as a shallow lake deposit (LE2). The second ca 200m thick unit is coarser and quartz-rich with some rare plant fragments. Several oxidized layers suggest pedogenesis in a humid climate. This unit is interpreted as a Hjulström-type fan delta deposit with strong sediment input (LE1). The following ca 150 m thick unit is a shallow lake desposit (LE2). As inferred from the geological map (Lasovskiy and Mozolev, 1961), the Jurassic is unconformably covered by ca 150 m of Paleocene to early Oligocene sediments corresponding to the Chonkurchak or Kokturpak Fm (Cobbold et al., 1994), of which only the upper 50 m are exposed. This unit of generally fine-grained sandstones contains numerous root traces and decimeter- to meter-thick caliche paleosols indicating very low sedimentation rates in a semi-arid environment. A meter-thick

layer of primary gypsum near the top might indicate evaporation in a large, shallow lake. This unit is interpreted as a distal alluvial plain deposit in a semi-arid climate (AP2a). The Paleogene series are unconformably covered by a massive, several hundred-meters thick conglomerate corresponding to the Oligocene – Miocene Kyrgyz and Shamsi formations (Lasovskiy and Mozolev, 1961). These deposits correspond to a proximal alluvial fan environment (AF1).

### 3.3. U-Pb (LA-ICP-MS) dating of apatite in the mafic sill

Apatite U-Pb dating of a mafic sill (KS-103; N41°20'22.19", E72°11'51.36") in the Hodzhiabad Fm from the Tash-Komyr section (Fig. 3) was carried out in the LA-ICP-MS facility at the laboratory of Géosciences Rennes, following the procedures described in Pochon et al. (2016). Information about sample preparation and instrumental conditions are reported in Supplementary Data B. The McClure ( $523.51 \pm 2.09$  Ma; Schoene and Bowring, 2006) and Durango ( $31.44 \pm 0.18$  Ma; McDowell et al., 2005) apatite secondary standards were used to control the accuracy of the analyses and consistently yielded  $^{207}\text{Pb}$  corrected ages of respectively  $525.9 \pm 7.5$  Ma (MSWD = 0.19; N = 4) and  $31.89 \pm 0.85$  Ma (MSWD = 2.1; N = 5) throughout the analyses. The apatite U-Pb LA-ICP-MS results can be found in Supplementary Data C. The twenty analyzed apatite grains yield a lower intercept age in a Tera-Wasserburg diagram of  $144.1 \pm 8.1$  Ma (MSWD=1.5) or  $144.0 \pm 8.1$  Ma (MSWD=1.5), if the initial common Pb value is forced to a  $^{207}\text{Pb}/^{206}\text{Pb}$  value of 0.845 ( $\pm 12\%$ ) calculated according to the Pb evolution model of Stacey and Kramers (1975) for an age of 140 Ma. As demonstrated by the numerical models of Pochon et al. (2016), solidification and cooling of these small volume mafic sills is very fast (< one century). Therefore, we can assume that the  $144 \pm 8$  Ma age represents the emplacement age for this sill.

### 3.4 Detrital zircon U-Pb dating

Zircon grains were separated using conventional magnetic and heavy liquid techniques, handpicked, mounted in one-inch epoxy resin pucks and polished to expose an internal section of the grains. Biasing of selected grains was kept to a minimum by randomly selecting grains with different shapes, size (63-250  $\mu\text{m}$ ) and color (Sláma and Kosler, 2012). Zircon grains were imaged for their cathodoluminescence (CL) properties using a Reliotron CL system equipped with a digital color camera. Based on CL-imaging, homogeneous zones within the crystals were selected for analysis to avoid mixing age domains. CL-images are also useful to extract petrogenetic information, such as textures indicative of an igneous or metamorphic origin, or thermal recrystallization domains (e.g. Corfu et al., 2003, Nasdala et al., 2003).

Zircon U-Pb analyses were mainly carried out at the LA-ICP-MS facility of the laboratory of Géosciences Rennes following the procedures described below and listed in Supplementary Data B. Three additional samples (SK-39B, SK-40 and SK-42) were analyzed at the University of Adelaide, following the procedures described in Lloyd et al. (2016). In Rennes, ablation was performed using an ESI NWR193UC Excimer laser, operating at 193 nm wavelength, connected to an Agilent 7700x quadrupole ICP-MS. In Adelaide, a New Wave UP-213 laser connected to an Agilent 7500 ICP-MS was used. Laser spot diameters between 22 and 30  $\mu\text{m}$ , with repetition rates of 3–5 Hz, were used for ablation. Data reduction was carried out with the GLITTER software (van Achterbergh et al., 2001). The raw data were corrected for Pb/U and Pb/Th laser-induced elemental fractionation and for instrumental mass discrimination by standard bracketing with repeated measurements of the zircon reference material GJ-1 (Jackson et al., 2004). No common Pb correction was applied. Along

with the unknowns, the Plešovice zircon standard was measured to monitor the accuracy and yielded a concordia age of  $337.3 \pm 0.6$  Ma (N=195), which is in good agreement with the reported ID-TIMS age of  $337.1 \pm 0.4$  Ma (Sláma et al., 2008). Ages were calculated using the Isoplot software (Ludwig, 2003). Further information on the instrumentation and analytical protocol used at Géosciences Rennes is detailed in Manzotti et al. (2015) and the protocol used in Adelaide in Payne et al. (2008). In this study, single-spot age results are given as  $^{207}\text{Pb}/^{206}\text{Pb}$  ages for results  $\geq 1$  Ga and as  $^{206}\text{Pb}/^{238}\text{U}$  ages for results  $< 1$  Ga. The complete isotopic dataset and single-spot age results can be found in Supplementary Data D.

The analyzed zircon grains vary in morphology from rounded to euhedral and from elongated to more stubby, equant shapes. The CL properties vary from grain to grain with internal oscillatory zoning or broad patchy zoning with or without bright rims to more homogeneous bright or dark grains with no visible internal structure. In a few grains, a core - rim distinction was visible. The Th/U ratios provide first-order information on the origin of the crystals (Fig. 6). In general, most detrital zircon grains seem to originate from igneous sources, although the Th/U ratio should be used with care to discriminate between igneous and metamorphic sources (e.g. Hoskin and Ireland, 2000).

In the following paragraphs, the numerical results obtained for all analyses are listed. No correlation was found between the obtained U-Pb ages, Th/U ratios and CL properties. Single-spot ages with 90-110% concordance are plotted as Kernel Density Estimation (KDE) diagrams using DensityPlotter (Vermeesch, 2012; Vermeesch et al., 2016) (Figs. 7; 8). The concordance filter is calculated using the formula  $100 * ((^{207}\text{Pb}/^{235}\text{U}) / (^{207}\text{Pb}/^{206}\text{Pb}))$  for single-spot ages  $> 1$  Ga, and using  $100 * ((^{206}\text{Pb}/^{238}\text{U}) / (^{207}\text{Pb}/^{235}\text{U}))$  for ages  $< 1$  Ga. A major peak refers to age populations including at least 40% of the total number of concordant spot ages, whereas we define a

minor peak as representing between 5% and 40% of the total number of concordant spot ages. In addition, a non-metric multidimensional scaling (MDS) diagram is made in order to visualize the 'dissimilarities' between the detrital age distributions (Fig. 9; Vermeesch, 2013; Vermeesch et al., 2016). In this diagram, less dissimilar samples plot closer together and the closest and second-closest neighbor are indicated with a solid and dashed line respectively.

### 3.4.1 Fergana Basin

#### *Tash-Komyr section*

Six Jurassic to Paleogene sandstones from the Tash-Komyr section were analyzed (Figs. 3; 6; 7; 8; Table 1). In the MDS diagram (Fig. 9) these six samples are distributed over two clusters, one including the samples KS-101 and KS13-13 (characterized by a closest neighbor relationship) and one including KS13-14, KS13-16, KS13-17 and KS13-18 (characterized by closest and second closest neighbor relationships).

Jurassic sample KS-101 yields 13% Precambrian ages between 760 and 2414 Ma, with Th/U ratios of 0.34 to 1.49. Paleozoic ages (87%) range from 285 to 475 Ma, with Th/U ratios of 0.18 to 1.01, and exhibit two major age groups: ca 400-475 Ma and ca 285-360 Ma.

Jurassic-Cretaceous sample KS13-13 contains 25% Precambrian ages from 635 to 2632 Ma with Th/U ratios of 0.01 to 5.69; 68% Paleozoic ages from 265 to 504 Ma, with age peaks around 300 Ma, 335 Ma, 400 Ma, and 440 Ma; 1.5% Middle Triassic ages from 234 to 244 Ma; and 5.5% Middle Jurassic ages from 165 to 174 Ma, suggesting a maximal depositional age of ca 165 Ma. For the Paleozoic and Mesozoic ages, Th/U ratios vary from 0.19 to 1.76.

Cretaceous sample KS13-14 yields 16% Precambrian ages between 799 and 2520 Ma with Th/U ratios of 0.05 to 1.00; and 84% Paleozoic ages between 261 and 480 Ma with Th/U ratios of 0.25 to 1.35. The Paleozoic ages exhibit two age groups: a major group ca 420-460 Ma and a minor group ca 285-320 Ma.

Paleogene sample KS13-16 yields 6.5% Precambrian ages from 798 to 1037 Ma with Th/U ratios of 0.12 to 0.93; 93.5% Paleozoic ages from 297 to 463 Ma with Th/U ratios of 0.24 to 3.36. The Paleozoic ages exhibit two age groups: a major group ca 400-463 Ma and a minor group ca 294-306 Ma.

Paleogene sample KS13-17 yields Precambrian ages (19%) from 638 to 2678 Ma with Th/U ratios of 0.03 to 1.12; Paleozoic ages (80%) from 295 to 465 Ma with Th/U ratios of 0.32 to 1.32; and 1 grain of  $46.7 \pm 0.6$  Ma (Lutetian) with a Th/U ratio of 0.64. There are two Paleozoic age groups: a major group ca 380-465 Ma and a minor group ca 295-310 Ma. In order of an age to be considered meaningful, a sample should yield at least three concordant grains of the same age within error. This is not the case for the one Lutetian zircon. Nevertheless, this age is consistent with the early Eocene depositional age estimated for this part of the section based on oyster fossils in a comparable section in the southwestern Tarim Basin (Bougeois et al., 2014; Bosboom et al., 2015).

Paleogene sample KS13-18 is the youngest sample from the section and yields 5% Precambrian ages between 547 and 2221 Ma with Th/U ratios of 0.22 to 0.66; 95% Paleozoic ages between 296 and 490 Ma with Th/U ratios of 0.30 to 1.20. The Paleozoic ages show two age groups: a major group ca 400-460 Ma and a minor group ca 296-315 Ma.

In general, in each Tash-Komyr sample, individual Precambrian ages range from 547 to 2520 Ma and vary in proportion from 5% (KS13-18) to 25% (KS13-13). A major Paleozoic population with a peak around 430 Ma and individual ages between 390 and 470

Ma is clearly present in all samples (ca 40% to 85% of the data; Figs. 7; 8). On the stacked normalized KDE plots it is clear that this age group is more abundant in the Paleogene samples compared to the Jurassic and Cretaceous samples (Fig. 8). Another Paleozoic age group of 270-315 Ma, is also present in all samples (ca 5% to 50% of the data). This group is clearly more important in the Jurassic - Cretaceous samples compared to the Paleogene samples (Figs. 7; 8). Noteworthy is that KS-101 and KS13-13 also contain zircon grains with ages between 315 and 360 Ma, which fall outside the two aforementioned Paleozoic age groups (Fig. 7). Minor (7%) Mesozoic (Middle Triassic and Middle Jurassic) ages were only found in KS13-13, but comparable ages are also found in samples of the Yarkand-Fergana Basin (see § 3.4.2; Fig. 7).

#### ***Jetim-Dobo section***

Five Jurassic to Paleogene sandstones were analyzed from the Jetim-Dobo section (Figs. 3; 6; 7; 8; Table 1). In the MDS diagram (Fig. 9), the samples show a large spread and are distributed over two clusters, one including the samples KS-119, KS13-01, KS13-02 and KS13-06 and one including KS13-10.

Jurassic *sample KS-119* yields 14% Precambrian ages from 612 to 2510 Ma with Th/U ratios of 0.21 to 1.16. The other 86% of the grains yield Paleozoic ages between 251 and 469 Ma with Th/U ratios of 0.17 to 0.97 and show two age groups, one minor group around 380-445 Ma and one major group around 260-300 Ma.

Jurassic–Cretaceous *sample KS13-01* yields 3.5% Neoproterozoic ages between 600 and 721 Ma (Th/U ratios of 0.22 to 0.72); 2.5% Mississippian ages between 330 and 336 Ma (Th/U ratios around 0.4); 93% Early-Middle Permian ages between 268 and 288

Ma (Th/U ratios of 0.35 to 0.76); and 1 grain with a Middle Jurassic age of  $166.1 \pm 2.0$  Ma (Th/U ratio of 0.72), showing oscillatory zoning.

Jurassic–Cretaceous *sample KS13-02* yields 14% Precambrian ages between 600 and 2640 Ma (Th/U ratios of 0.04 to 1.98); 85% Paleozoic ages between 265 and 489 Ma (Th/U ratios of 0.09 to 0.96); and 1 grain with a Middle Jurassic age of  $167.7 \pm 2.1$  Ma (Th/U ratio of 0.63), showing bright internal oscillatory zoning.

From Cretaceous *sample KS13-06*, 31% of the analyzed grains are Precambrian from 827 to 2498 Ma with Th/U ratios of 0.11 to 1.52. Paleozoic (66%) and Mesozoic (3%) ages vary from 240 to 447 Ma with Th/U ratios of 0.05 to 1.51. Two major age groups can be identified: ca 405–445 Ma and ca 260–310 Ma.

Paleogene *sample KS13-10* yields Precambrian ages (13.5%) from 650 to 2520 Ma with Th/U ratios of 0.16 to 1.62; and Paleozoic ages (86.5%) from 270 to 505 Ma with Th/U ratios of 0.25 to 1.12, showing a major age peak around 440 Ma.

In general, in each Jetim-Dobo sample, individual Precambrian ages range from 612 to 2640 Ma and vary in proportion between 3% (KS13-01) and 31% (sample KS13-06). Comparable to the Tash-Komyr section, the early Paleozoic (390–470 Ma) age group is present in most samples (6–80% of the data), except for KS13-01 (Figs. 7; 8). Again, this age group is more abundant in the Upper Cretaceous and Paleogene samples. The Late Paleozoic (260–315 Ma) age group is present in every sample as well, but is most dominant in KS13-01 and KS13-02 (ca 93% of the grains) (Figs. 7; 8). It is interesting to note that samples KS13-01 and KS13-02 also contain zircon grains with ages between 315 and 340 Ma, which fall outside the two major Paleozoic age groups (Fig. 7). Finally, three samples contain small amounts of Mesozoic zircon grains (Fig. 7). Sample KS13-06 yields two Middle Triassic ages (ca 240 Ma), and KS13-01 and KS13-02 each contain one Middle Jurassic grain of 166 and

168 Ma respectively. These three samples do not fulfill the condition of minimal three concordant grains of the same age within error, but the Middle Jurassic ages are indicative for a maximal depositional age of ca 167 Ma for this part of the section. In general, these Mesozoic ages are comparable to those in sample KS13-13 from Tash-Komyr (§ 3.4.1) and in KS13-20 and KS13-22 from the Yarkand-Fergana Basin (§ 3.4.2).

### 3.4.2 Yarkand-Fergana Basin

From the Terek section, two Jurassic and Cretaceous sandstones (*KS-106* and *KS-113* respectively) were analyzed (Figs. 4; 6; 7; 8; Table 1). In the MDS diagram, these samples plot close together and are characterized by a closest neighbor relationship (Fig. 9). Precambrian ages are abundant (32 to 37%), varying from 685 to 2840 Ma and mainly distributed in three minor groups (700-900 Ma, 1750-1950 Ma, and 2350-2500 Ma) with Th/U ratios between 0.08 and 5.75. Paleozoic ages (58 to 61%) range between ca 255 and 470 Ma, and two minor age peaks (275 Ma and 430 Ma) can be identified. Triassic ages (4.5 to 6%) vary from 215 to 250 Ma and one grain in *KS-113* yields a Late Jurassic – Early Cretaceous age of  $145.7 \pm 1.7$  Ma. Th/U ratios for the Paleozoic and Mesozoic ages range from 0.01 to 1.48, but most are  $> 0.3$ .

From additional outcrops in the Yarkand-Fergana Basin (Figs. 2; 6; 7; 8; Table 1) sample *KS13-22* was taken along the Chitty river and belongs to the Early-Middle Jurassic (Belgovskiy et al., 1958; Genkina, 1977). This sample shows a second-closest neighbor relationship with sample *KS-113* from the Terek section in the MDS diagram (Fig. 9). Precambrian ages (4%) range from 802 to 1674 Ma (Th/U ratios of 0.31 to 0.80), Paleozoic ages (47%) range between 254 and 514 Ma (Th/U ratios of 0.14 to 1.52), Early to Late Triassic ages (6%) range between 210 and 250 Ma (Th/U ratios of 0.37 to 0.86), and Early-

Middle Jurassic ages (43%) range between 160 and 190 Ma (Th/U ratios of 0.17 to 1.08, and mostly  $> 0.3$ ). The Early -Middle Jurassic ages form a major age peak in the KDE plot and suggest a maximal depositional age of ca 160 Ma (Fig. 7). Along the Yassy river, the Jurassic - Cretaceous transition is marked by a thick conglomerate, similar to the Tash-Komyr section. A fine-grained Jurassic sandstone (*sample KS13-20*) from the lower part of this alluvial fan system shows a closest neighbor relationship with KS13-22 in the MDS diagram (Fig. 9) and yields 20% Precambrian ages between 568 and 2536 Ma (Th/U ratios of 0.32 to 1.06), 70% Paleozoic ages between 278 and 487 Ma (Th/U ratios of 0.17 to 1.38) with a minor age group ca 380-490 Ma and a major group ca 280-320 Ma; and 10% Early-Middle Jurassic ages between 167 and 182 Ma, implying a maximal depositional age of ca 167 Ma (Figs. 6; 7; 8).

### 3.4.3 Issyk-Kul Basin

Three Jurassic sandstone samples from the Kadji-Sai section in the Issyk-Kul Basin were analyzed: *SK-39B*, *SK-40* and *SK-42* (Figs. 5; 6; 7; 8; Table 1). These samples plot closely together in the MDS diagram (Fig. 9). *Sample SK-39B* yields 14% Neoproterozoic ages between 589 and 950 Ma with Th/U ratios of 0.11 to 0.32; 86% Paleozoic ages between 348 and 512 Ma with Th/U ratios of 0.03 to 1.31 and exhibiting a major peak around 420 Ma. No Permian or younger ages were found. *Sample SK-40* yields 5% Proterozoic ages ranging between 592 and 2122 Ma with Th/U ratios of 0.03 to 0.76; 95% Paleozoic ages between 289 and 478 Ma with Th/U ratios of 0.13 to 1.32. Two Paleozoic age groups can be identified: a major group ca 390-480 Ma and a minor group ca 290-320 Ma. *Sample SK-42* yields 7% Proterozoic ages between 756 and 1690 Ma with Th/U ratios of 0.26 to 0.52; 93% Paleozoic ages between 287 and 472 Ma with Th/U ratios of 0.25 to 1.40 and two age groups: a major group ca 400-480 Ma and a minor group ca 290-320 Ma.

## 4. Discussion

### 4.1 Potential sediment provenance

Potential sediment provenance is suggested based on a comparison of the detrital zircon U-Pb results (Figs. 7; 8; 9) with available zircon U-Pb data on basement rocks (Fig. 2) and published detrital zircon U-Pb studies in the Tien Shan.

The Precambrian U-Pb ages found in all samples show a large spread (Fig. 7). Nevertheless, some recurrent age groups can be identified at 750-950 Ma and, with a smaller amount of data, at 1750-2000 Ma and 2400-2600 Ma. Comparable detrital and single grain zircon U-Pb ages were found in the NTS, MTS and STS as well as in the Chinese South Tien Shan, the northern Pamir and the Tarim craton (Brookfield, 2000; Ren et al., 2011; Shu et al., 2011; Bershaw et al., 2012; Carroll et al., 2013; Kröner et al., 2013; 2017; Liu et al., 2013; Yang et al., 2013; Rojas-Agramonte et al., 2014; Han et al., 2015; Konopelko et al., 2015; 2017a; Käßner et al., 2016; Konopelko and Klemd, 2016; Kröner et al., 2017; Worthington et al., 2017). The Precambrian U-Pb ages found in our samples either reflect a direct link with Precambrian units and/or a recycling of sediments containing those Precambrian zircon grains.

Paleozoic U-Pb ages from the detrital samples can be generally divided in two main age groups, a “Caledonian” and a “Hercynian” one (Figs. 7; 8), following the traditional terminology (e.g. Konopelko et al., 2007). The Caledonian group is defined by Early-Middle Ordovician to Early-Middle Devonian ages (470-390 Ma), with a peak around 440-420 Ma. This group is clearly present in all studied sections. Granitoids with similar ages are widespread in the NTS, and to a minor extent in the MTS (e.g. Chatkal, Bozbutau, Atbashi ranges with ages between 467 and 410 Ma; Alexeiev et al., 2016; Konopelko et al., 2017b;

Macaulay et al., 2016 and references therein) (Fig. 2). They can be related to arc and collisional magmatism reflecting the Early Ordovician to Middle Devonian amalgamation history of the NTS and MTS to the Kazakhstan paleocontinent (e.g. Konopelko et al., 2008; 2017b; Glorie et al., 2010; Alexeiev et al., 2011; 2016; De Grave et al., 2011; 2013; Seltmann et al., 2011). Ordovician to Middle Devonian U-Pb ages of igneous and detrital zircons are reported from the Yili-Central and South Tien Shan in NW China (Ren et al., 2011; Liu et al., 2013; Yang et al., 2013; Han et al., 2015, 2016), the West Junggar and northern Balkhash mountains in Kazakhstan (Kröner et al., 2008; Wang et al., 2012); and in the North and Central Pamir (Schwab et al., 2004).

The younger Paleozoic, Hercynian, age group is present in most samples (Figs. 7; 8) and is characterized by ages between 315 and 260 Ma (west of the TFF) and between 315 and 290 Ma (east of the TFF). In the STS, Early Permian granitoids are widespread, whereas Pennsylvanian zircon ages are reported from the Gissar mountain range (Konopelko et al., 2007; 2009; 2017b; Seltmann et al., 2011; De Grave et al., 2012; Käßner et al., 2016 and references therein; Worthington et al., 2017) (Fig. 2). In the MTS and NTS, Pennsylvanian – Early Permian ages are mainly reported from the Chatkal-Kurama mountain ranges and Hercynian granitoids also occur to a minor extent in mountain ranges adjacent to the Naryn and Issyk-Kul basins (Alekseev et al., 2009; Glorie et al., 2010; De Grave et al., 2011; Seltmann et al., 2011; Macaulay et al., 2016 and references therein; Konopelko et al., 2017b; Worthington et al., 2017) (Fig. 2). In the Chinese North, Yili-Central and South Tien Shan, in the West Junggar and northern Balkhash (Kazakhstan) regions, late Paleozoic ages occur as well (Seltmann et al., 2011; Shen et al., 2013; Chen et al., 2015; De Pelsmaecker et al., 2015). In general, these Hercynian ages reflect the late Paleozoic assembly of the ancestral Tien Shan and can be linked to arc and (post-) collisional magmatism related to the closure of the

Turkestan and Junggar-Balkhash oceans and/or to the Kazakhstan - Tarim collision (e.g. Konopelko et al., 2007; 2015; Windley et al., 2007; Alekseev et al., 2009; Seltmann et al., 2011; Liu et al., 2013, 2014; Alexeiev et al., 2016; Safonova et al., 2016). In several samples (KS13-01; KS13-02; KS-106; KS-113; KS13-13; KS13-22) ages ranging from 360 to 315 Ma occur as well (Figs. 7; 8). Similar ages are also found in detrital samples from the southern Junggar Basin (Yang et al., 2013) and in the Chinese Central and South Tien Shan (Ren et al., 2011; Liu et al., 2013; Han et al., 2015, 2016). U-Pb ages of igneous rocks between ca 360-315 Ma are reported from the Yili belt (e.g. Han et al., 2006; Tang et al., 2010; Shen et al., 2012; Xiao et al., 2013; De Pelsmaeker et al., 2015), the Chinese Central Tien Shan (Tang et al., 2010; Käßner et al., 2016 and references therein), the Gissar-Alai Range (Käßner et al., 2016 and references therein) and from the Trans-Alai range in the northern Pamir (Schwab et al., 2004; Sun et al., 2016).

Triassic ages are found in several detrital samples west of the TFF: KS13-06 and KS13-13 (ca 234 -244 Ma) from the Fergana Basin; and KS13-22, KS-106 and KS-113 (ca 250-210 Ma) from the Yarkand-Fergana Basin (Fig. 7). Triassic zircon U-Pb basement ages are rarely recognized in the Tien Shan, but Seltmann et al. (2011) reported a Triassic thermal event in the Kyzylkum segment of the STS in Uzbekistan around 240-220 Ma. Käßner et al. (2016) reported Triassic  $^{40}\text{Ar}/^{39}\text{Ar}$  ages (ca 256-238 Ma) in the Gissar Range related to small-volume basanite magmatism. Another possible source area is situated in the northern Pamir where several authors reported the existence of Triassic to Early Jurassic granitic plutons (e.g. Robinson et al., 2004; Bershaw et al., 2012; Angiollini et al., 2013; Robinson, 2015). Schwab et al. (2004) also dated a large batholith close to Karakul lake in the Pamir at ca 225 Ma. Triassic detrital zircon U-Pb ages are reported by Worthington et al. (2017) in a Cretaceous sample south of the Garm massif; by Bershaw et al. (2012) and Sun et al. (2016)

for Meso-Cenozoic samples close to the Main Pamir Thrust and western Tarim Basin and by Liu et al. (2013), Jia et al. (2015) and Han et al. (2016) in Meso-Cenozoic samples in the piedmont of the STS in NW China.

Early and Middle Jurassic ages are found in several samples west of the TFF: KS13-13; KS13-01 and KS13-02 (ca 165-174 Ma) from the Fergana Basin; and KS13-20 and KS13-22 (ca 160-190 Ma) from the Yarkand-Fergana Basin (Figs. 7; 8). These ages are only present in samples with a Jurassic - Early Cretaceous depositional age and are not found in the analyzed samples with younger stratigraphic ages. The Th/U ratios for the zircon grains of this age group range between 0.28 and 1.76 (Fig. 6) and CL images often show oscillatory zoning, indicative of a magmatic origin. Because of the limited difference between the depositional age and detrital zircon ages for some of the samples, it is likely that the grains mostly come from igneous sources. Further we cannot exclude that these zircon grains represent a volcanoclastic component. Jurassic igneous rocks are not widely reported in the Tien Shan, but early Mesozoic tuffaceous sandstones and detrital Jurassic - Early Cretaceous ages in Meso-Cenozoic samples are found in the Junggar Basin and piedmont of the STS in NW China, suggesting the possibility of volcanism distributed along major fault zones during the Early-Middle Jurassic (Simonov et al., 2008; 2015; Yang et al., 2013, 2014; Fang et al., 2015; Jia et al., 2015). According to Shlezinger (1971), dykes occasionally occur in the Jurassic deposits of the Yarkand-Fergana Basin. Also Rolland et al. (2013) reported an  $^{40}\text{Ar}/^{39}\text{Ar}$  age of ca 195 Ma on muscovite from a pegmatite dyke in the Fergana Range along the TFF. In addition, a possible source area outside the Tien Shan is situated in the Central - Southern Pamir, where Jurassic-Early Cretaceous arc volcanism and collisional granitoids are reported (Fraser et al., 2001; Ducea et al., 2003; Schwab et al., 2004; Bershaw et al., 2012; Robinson, 2015) (Fig. 2).

## 4.2 Jurassic to Paleogene paleogeographic and tectonic implications

### 4.2.1 Early – Middle Jurassic

In the Kadji-Sai and Ming-Kush sections, Lower-Middle Jurassic fluvial to shallow lake deposits with a maximum thickness of a few hundred meters unconformably overlie Paleozoic basement (Figs. 2; 5). The sediments in both sections include organic-rich layers and plant remnants, suggesting humid climate conditions during deposition. The three Jurassic samples (SK-39B/40/42) of the Kadji-Sai section show very similar detrital age spectra (Figs. 7; 8), and plot close together in the MDS diagram (Fig. 9). These age spectra are also very similar to those of Jurassic-Paleogene samples from Jeti-Oguz and Chon Kyzylsu south of lake Issyk-Kul (Macaulay et al., 2016). The dominant Caledonian zircon age group (390-480 Ma) and limited Hercynian ages can be attributed to a NTS - MTS provenance, with almost no influence of the Yili belt (Fig. 2; §4.1). This suggests the existence of an uplifted NTS-MTS south of the present-day Issyk-Kul Basin (Fig. 10). Macaulay et al. (2016) suggest a similar drainage divide during the Cenozoic with a NTS (Terskey Range) provenance for the sediments of the southern Issyk-Kul Basin.

In the Fergana Basin, a more complete Lower-Middle Jurassic sedimentary record exists. In the Tash-Komyr section the sediments consist of shallow lake, fan delta to distal alluvial plain deposits including plant remnants and coal layers, indicating deposition in a humid climate (Fig. 3). In the Jetim-Dobo section, the organic-rich (including coal seams) Lower-Middle Jurassic sediments also suggest humid climate conditions (Fig. 3). Comparable Lower-Middle Jurassic continental sediments were deposited in the Alai Basin, south of the Fergana Basin, at the periphery of the area under marine influence in the Tajik depression (Coutand et al., 2002; Fig. 2). The detrital age spectra for both Lower-Middle Jurassic

samples from the Fergana Basin (KS-101 from Tash-Komyr and KS-119 from Jetim-Dobo), show broad Caledonian and Hercynian age groups, the latter including Mississippian ages (Figs. 7; 8). These results, together with the low-energy depositional environment, suggest a relatively large drainage system whereby a combination of the NTS, MTS or STS signals contributed to the age distribution (Fig. 10). Our results are in agreement with the study of Li et al. (2004), Liu et al. (2013), and Yang et al. (2014) showing that the basin-range pattern in the central and south(western) Tien Shan in NW China was characterized by a large geographic source area and a decreasing topography from the Late Permian until the Early Jurassic based on detrital zircon, compositional maturity and heavy mineral studies of the sedimentary record. These findings are consistent with the general planation that affected most of Central Asia, including the Tien Shan, during the Late Triassic – Early Jurassic (e.g. Clarke, 1984; Bebeshev, 1995; Jolivet et al., 2007; Jolivet, 2015), and with thermochronological data that show a slow basement cooling during most of the Jurassic after a Late Triassic - Early Jurassic cooling signal based on data from the Song-Kul plateau, the Alai, Trans-Alai and Terskey ranges and from the central and western Chinese Tien Shan (e.g. Dumitru et al., 2001; Sobel et al., 2006b; Jolivet et al., 2010; De Grave et al., 2011, 2012; Tang et al., 2015; Glorie and De Grave, 2016; Zhang et al., 2016; Gillespie et al., 2017; Wang et al., 2017).

In the Yarkand-Fergana Basin, the Lower-Middle Jurassic sediments are intense deformed compared to the sediments in the Fergana Basin and are mostly represented by lacustrine flash-flood and shale deposits. In the Terek section, following the basal, few meters thick alluvial fan, the sediment facies correspond to Hjulström-type fan delta and lake environments (Fig. 4). These deeper depositional environments compared to the contemporaneous shallow lake, fan delta to distal alluvial plain deposits of the Fergana

Basin, suggest that the strongest subsidence occurred in the Yarkand-Fergana Basin, in agreement with the interpretation of an active transtensional pull-apart regime for the basin during the Early-Middle Jurassic (Burtman et al., 1996; Sobel, 1999; Allen et al., 2001; Alexeiev et al., 2017). In both Lower-Middle Jurassic samples (KS-106 and KS13-22) from the Yarkand-Fergana Basin, Caledonian (420-440 Ma), Hercynian (260-290 Ma) and minor Triassic (210-250 Ma) zircon age groups can be identified (Figs. 7; 8). The major (43%) Early-Middle Jurassic (160-190 Ma) age peak in sample KS13-22 with a putative depositional age around the Middle-Late Jurassic boundary suggests a short lag time (Fig. 7). The provenance of the Early-Middle Jurassic zircon grains can possibly be linked to volcanism distributed along major faults in the Tien Shan at that time (Shlezinger, 1971; Simonov et al., 2008; Yang et al., 2013, 2014; Fang et al., 2015; Jia et al., 2015; Jolivet, 2015; § 4.1). Volcanism could be generated and channeled along the TFF - which was active during that time - and could act as a local source for syn-sedimentary zircon grains in the Yarkand-Fergana Basin. Another possible, but more distal, source area is located in the present-day Pamir, where Triassic and Jurassic igneous rocks are reported (Fig. 2; § 4.1). Minor Triassic and Jurassic U-Pb ages are also found in Meso-Cenozoic samples in the piedmont of the STS in NW China from detrital zircon studies of Liu et al. (2013) and Jia et al. (2015). An uplifted northern Pamir is put forward by Robinson (2015) and is consistent with the studies from Sobel and Dumitru (1997), and Bershaw et al. (2012), that show that Jurassic sediments of the NW Tarim Basin were mainly derived from the northern Pamir.

#### **4.2.2 Late Jurassic - Early Cretaceous**

In the Fergana and Yarkand-Fergana basins west of the TFF Upper Jurassic – Cretaceous sediments occur, in contrast to the studied basins east of the TFF where no

Upper Jurassic – Cretaceous sediments are deposited or preserved (Kuzichkina, 1972). Note that some Jurassic - Lower Cretaceous sediments locally occur in the Toyun Basin, east of the TFF in the extension of the Yarkand-Fergana Basin (Sobel and Arnaud, 2000; Li and Xu, 2007).

From both sections in the Fergana Basin, the Jurassic – Cretaceous transition is most outspoken in the Tash-Komyr section. There, the transition is characterized by an erosional unconformity between a distal alluvial plain facies and a well-developed alluvial fan system consisting of a >110m thick conglomerate (Hodzhiabad Fm) (Fig. 3). Based on the  $144 \pm 8$  Ma apatite U-Pb age of the mafic sill intruded in the conglomerate (§ 3.3) and the early Oxfordian maximum age suggested for the Balabansay Fm (Belgovskiy et al., 1958; Kuzichkina, 1972; Aliev et al, 1981), the age of the Hodzhiabad Fm can be constrained to Oxfordian - Valanginian. Comparable well-developed alluvial fan systems have also been observed in the northern and southern piedmonts of the Chinese Tien Shan (Kalaza Fm; Jolivet et al., 2013b; 2015; Fang et al., 2015). The geodynamic significance of these conglomerates is still highly debated. Evidence for Late Jurassic – Early Cretaceous deformation and metamorphism have been reported from the West Kunlun ranges and the Pamir (e.g. Arnaud et al., 1993). In the southern Junggar Basin, an angular unconformity has been reported at the base of the Kalaza Fm, indicating tectonic movement during the Late Jurassic – Early Cretaceous (Hendrix et al., 1992; Eberth et al., 2001). An active tectonic setting is further attested by continuous sediment recycling along the southern margin of the Junggar Basin during the same period (Yang et al., 2013). However, Jolivet et al. (2015) recently proposed that in the south Junggar and Tarim basins, the alluvial fans of the Kalaza Fm represent the proximal facies of a hyper-arid sequence characterized by large aeolian dunes in the distal parts of the system. Paleocurrents are mostly E-SE directed in the Lower Cretaceous series, which is very different from the generally W-directed paleocurrents in the

Upper Jurassic sediments, indicating a change in provenance. The authors suggest that the sudden occurrence of coarse sediment could be related to a sudden change in climate in a continuously active tectonic framework. In both the Tash-Komyr and Jetim-Dobo sections, shallow lake, Hjulström-type fan delta and distal alluvial plain deposits occur above the alluvial fan facies (Fig. 3). The absence of organic-rich sediments in all sections, together with the presence of abundant calcareous paleosols in the Lower Cretaceous sediments in Tash-Komyr, indicates a change from humid to semi-arid climate conditions (Fig. 3). This climate change from humid during the Early-Middle Jurassic to semi-arid during the Late Jurassic - Early Cretaceous is consistent with published data from sedimentary basins in and near the Tien Shan (e.g. Clarke, 1984; Graham et al., 1990; Allen et al., 1991; Hendrix et al., 1992; Bebeshev, 1995; Hendrix, 2000; Eberth et al., 2001; Jolivet et al., 2015) and possibly initiated before the deposition of the Hodzhiabad Fm as indicated by the occurrence of small calcareous nodules in the underlying Upper Jurassic alluvial plain deposit in Tash-Komyr (Fig. 3).

In the Yarkand-Fergana Basin, the Jurassic - Cretaceous transition was studied along the Yassy river and in the Terek section (Figs. 2; 4). Along the Yassy river, the transition is characterized by a thick conglomerate, comparable to the well-developed alluvial fan system described in Tash-Komyr. In Terek, the Jurassic-Cretaceous transition is characterized by a change from shallow most distal lake, over proximal alluvial fan to Hjulström-type fan delta deposits (Fig. 4). The sediments represent a shallower depositional environment compared to the Early-Middle Jurassic setting. During the Cretaceous, the depocentre also extended more to the southwest of the basin (Belgovskiy et al., 1958; Genkina, 1977).

From the Fergana and Yarkand-Fergana basins, detrital zircon U-Pb data were obtained from five Upper Jurassic – Lower Cretaceous samples: KS13-13 and KS13-14 (Tash-

Komyr); KS13-01 and KS13-02 (Jetim-Dobo); and KS13-20 (Yassy river) (Figs. 4; 6; 7; 8). Sample KS13-13 is stratigraphically below the Hodzhiabad Fm and contains 68% Paleozoic (265-504 Ma); 1.5% Middle Triassic (244-234 Ma) and 5.5% Middle Jurassic (165-174 Ma) ages. In the younger Cretaceous sample KS13-14 from Tash-Komyr, Caledonian (420-460 Ma) and Hercynian (285-320 Ma) age groups are clearly present, but no Mesozoic ages have been found (Fig. 7). Sample KS13-01 from Jetim-Dobo contains a few (3.5%) Precambrian ages, a few (2.5%) Mississippian ages and a very large group (93%) of Early-Middle Permian ages (Fig. 7). This remarkable age distribution, with no Caledonian ages, is also reflected in the MDS diagram (Fig. 9) and suggests a small drainage system with most of the material being derived from a Permian intrusive body, likely from the MTS or STS, as primary source. Sample KS13-02 is located ca 50m higher in the section and forms the closest neighbor and second-closest neighbor in the MDS diagram with samples KS13-22 and KS13-01 respectively (Fig. 9). Besides abundant Hercynian ages (78.5%; 265-325 Ma), the age spectrum exhibits a slight increase in the amount of Precambrian (14%) and Caledonian ages (6.5%; 397-489 Ma) compared to KS13-01 (Fig. 7). This suggests a similar, but slightly larger drainage system compared to KS13-01. The almost complete absence of Caledonian ages for KS13-01 and -02 from Jetim-Dobo and the narrower Caledonian and Hercynian age groups in all Upper Jurassic – Lower Cretaceous samples compared to the older Jurassic samples (KS-101, KS-119) suggest a smaller drainage system - probably related to some relief development localized along the TFF - during the Late Jurassic–Early Cretaceous compared to the Early-Middle Jurassic (Figs. 7; 8; 10). The detrital zircon U-Pb age distribution of KS13-20 (lower part of alluvial fan along the Yassy river) shows a minor Caledonian age group (380-490 Ma), a major Hercynian age group (280-320 Ma), and 10% Early-Middle Jurassic ages (167-182 Ma) (Figs. 7; 8). The presence of minor Mesozoic ages in the Upper Jurassic - Lower

Cretaceous samples from the Fergana (KS13-13, KS13-01, KS13-02) and Yarkand-Fergana basins (KS13-20) suggests potential recycling of the older Jurassic sediments from these basins and/or a minor influence of uplifted areas in the present-day Pamir region, which is consistent with the clustering of these samples in the MDS diagram (Fig. 9).

Based on (1) the shallower depositional environment compared to the Early-Middle Jurassic setting; (2) the extension of the depocentre more to the southwest of the basin during the Cretaceous; and (3) the detrital zircon U-Pb data showing recycling of older Jurassic sediments and smaller drainage systems compared to Early-Middle Jurassic settings, we suggest that by the Late Jurassic – Early Cretaceous the tectonic regime changed to a more compressive setting whereby the Yarkand-Fergana Basin was inverted. An inversion at the end of the Middle Jurassic is also documented in the Leontiev Graben and South Turgai basins along the TFF by an angular unconformity between the Middle and Upper Jurassic series (Yin et al., 2012; Alexeiev et al., 2017). The change in tectonic regime can be related to the collision-accretion event of South Pamir (Lhasa terrane)-Karakoram to Eurasia during the Late Jurassic–Early Cretaceous and the resultant rotational movements between Kazakhstan, Junggar, Tarim and Siberia (e.g. Robinson et al., 2004, Schwab et al., 2004; Choulet et al., 2013; Robinson, 2015; Gillespie et al., 2017).

Additional evidence for renewed tectonic activity and topography development can be found in thermochronological data of De Grave et al. (2012) and Glorie and De Grave (2016), who demonstrated a Late Jurassic - Early Cretaceous cooling event (ca 150-110 Ma) in the Kyrgyz Tien Shan basement. Coutand et al. (2002) further related the Lower Cretaceous coarse clastic deposits in the Alai Basin to a denudation event north of the basin and several authors proposed erosion of the Tien Shan blocks east of the TFF during that time (e.g. Hendrix et al. 1992; Sobel 1999; Hendrix, 2000; Yang et al. 2013; De

Pelsmaeker et al., 2015; Glorie and De Grave, 2016). The sandstone compositional data, heavy mineral and detrital zircon studies from Li et al. (2004) and Li and Peng (2010) along the northern margin of the Tarim Basin (Kuqa subbasin) also indicate renewed tectonic activity during that time. They also demonstrate, based on the remarkable increase of Hercynian ages in the detrital zircon age spectra, that Lower Cretaceous samples exhibit a new provenance supply resulting from denudation processes in the southern Tien Shan. In the Pamir region, Robinson (2015) suggested widespread deformation and significant crustal shortening during the Late Jurassic – Early Cretaceous.

#### **4.2.3 Late Cretaceous – early Paleogene**

In the Tash-Komyr section, the Upper Cretaceous sediments are represented by alluvial plain deposits intercalated with numerous calcareous paleosols (caliches and calcretes), suggesting no or very slow sedimentation but also no or very slow erosion (Fig. 3). In the Jetim-Dobo section, the Upper Cretaceous sediments are not very well exposed, but are mainly represented by alluvial plain and Hjulström-type fan delta deposits (Fig. 3), indicating significant subsidence in that part of the Fergana Basin. A few calcareous paleosols are observed towards the Paleogene transition (Fig. 3). In the Terek section, the Upper Cretaceous sediments are represented by alluvial plain deposits with no observation of calcareous paleosols, indicating stronger continuous sedimentation and possibly a more humid environment than in Tash-Komyr, but less subsidence than in Jetim-Dobo (Fig. 4). The lower Paleogene sediments in the Fergana Basin are mainly represented by alluvial plain deposits, intercalated with Hjulström-type fan delta deposits and a few marine incursions related to the proto-Paratethys Sea (Fig. 3; Bosboom et al., 2011; 2015). Also in the Yarkand-Fergana Basin, shallow marine incursions occurred during the early Paleogene (Heng-Ren et

al., 1983; Lee, 1985; Yichun et al., 1988; Dercourt et al., 1993). Furthermore, in the Alai Basin, marine transgressions occurred between the Cenomanian and Oligocene whereby the Tajik depression was connected to the western Tarim Basin (Burtman, 2000; Coutand et al., 2002) and probably also to the Fergana Basin (Fig. 10). The Upper Cretaceous - lower Paleogene sediments of the Yarkand-Fergana and Fergana basins differ significantly from the studied sections east of the TFF. In the latter, apparently no sedimentation took place during the Late Cretaceous and the area was likely characterized by a slowly eroding, relatively flat topography (Fig. 10). Sedimentation resumed during the early Paleogene with the deposition of continental red beds with subordinate lacustrine carbonates.

Detrital zircon U-Pb data was obtained from six Upper Cretaceous - lower Paleogene samples: KS-113 (Terek), KS13-06 and KS13-10 (Jetim-Dobo), and KS13-16, KS13-17 and KS13-18 (Tash-Komyr) (Figs. 6; 7; 8). The Cretaceous sample KS-113 from Terek displays a similar age spectrum compared to the older Jurassic sample KS-106 from the same section, a major Caledonian (420-440 Ma) and a minor Hercynian (260-290 Ma) age group and a few Triassic ages (6%; 224-250 Ma) (Figs. 7; 8), inducing a closest neighbor relation in the MDS diagram (Fig. 9). The age spectrum for the Cretaceous sample KS13-06 from Jetim-Dobo shows a major Caledonian (405-445 Ma), a major Hercynian (260-310 Ma) and a minor (3%) Triassic (ca 240 Ma) age group (Figs. 7; 8) and is comparable with the spectra for KS-106, KS-113 and KS13-13 as indicated in the MDS diagram (Fig. 9). These findings suggest that both age spectra for the Cretaceous samples KS-113 and KS13-06 can be explained by potential recycling of the older Jurassic-Cretaceous series. The three lower Paleogene samples from Tash-Komyr (KS13-16/17/18) show similar age distributions whereby the Paleozoic ages (80-93%) can be divided into two groups: a sharp and major Caledonian (390-465 Ma) and a minor Hercynian (285-320 Ma) one (Figs. 7; 8; 9). No Mesozoic or Cenozoic

ages were found. The Paleogene sample (KS13-10) from Jetim-Dobo shows a similar pattern where almost all of the Paleozoic ages are Caledonian with only a few Hercynian exceptions (Figs. 7; 8). In general, the age spectra of the Paleogene samples from Tash-Komyr and Jetim-Dobo are similar to those of the Cretaceous sample KS13-14 from Tash-Komyr and the Jurassic samples from Kadji-Sai (SK-39B/40/42) as shown in the MDS diagram (Fig. 9) and can be related to the limited presence of Pennsylvanian - Permian ages, reflecting that the sediments were mainly derived from NTS and MTS sources, without influence of the Yili belt. The almost complete absence of Pennsylvanian - Permian single-spot ages up-section suggests a change in topography whereby the drainage areas became broader towards the MTS and NTS during the Late Cretaceous – early Paleogene (Figs. 7; 8; 10). This result is consistent with the study of Yang et al. (2014) who report that the diversity of detrital zircon U-Pb ages reached a minimum in the Meso-Cenozoic sedimentation history during the Late Cretaceous. Our results support a paleogeographical setting where the Fergana, Yarkand-Fergana, Tajik and western Tarim basins were connected to each other – in agreement with earlier observations (e.g. Heng-Ren et al., 1983; Yichun et al., 1988) - and low-relief land area was located east of the TFF, where large Caledonian plutons are more prominent compared to the scattered Pennsylvanian-Permian granitoid bodies (Fig. 10).

## 5. Conclusion

a) During the Early-Middle Jurassic, the TFF was active and the strongest subsidence occurred in the Yarkand-Fergana Basin based on the depositional facies and sediment distribution patterns. The presence of Jurassic (190-160 Ma) and Triassic (250-210 Ma) detrital zircon ages besides Hercynian (315-260 Ma), Caledonian (470-390 Ma) and

Precambrian ages indicate that the Early-Middle Jurassic sediments were derived from a combination of local and distal sources. Local sources from syn-sedimentary volcanism along the TFF and elevated areas to the east of the TFF, and more distal sources to the (south)west of the TFF, possibly stretching into the present-day Pamir region. In the Fergana Basin, Early-Middle Jurassic low-energy deposits and a wide spectrum of Paleozoic (470-252 Ma) zircon ages suggest a large drainage system with provenance from either the NTS, MTS and STS. This is consistent with a decreasing topography related to a general planation of the Tien Shan during the Late Triassic – Middle Jurassic. In the Issyk-Kul Basin, the dominance of Caledonian (470-390 Ma) ages and limited presence of Hercynian ages in the Early-Middle Jurassic sediments indicate an uplifted NTS-MTS south of the present-day Issyk-Kul Basin. In all studied sections, coal layers and plant remnants point to a humid climate during the Early-Middle Jurassic.

b) During the Late Jurassic - Early Cretaceous, renewed compression led to the inversion of the Yarkand-Fergana Basin. The sediments represent a shallower depositional environment compared to the Early-Middle Jurassic setting and the presence of some Jurassic (190-160 Ma) and Triassic (250-215 Ma) detrital zircon ages in both Yarkand-Fergana and Fergana basins can be explained by recycling of older Jurassic series from the Yarkand-Fergana Basin and/or by a minor influence of uplifted areas in the present-day Pamir region. The almost complete absence of Caledonian (470-390 Ma) ages for the Upper Jurassic – Lower Cretaceous samples from Jetim-Dobo suggests a smaller drainage system compared to the Early-Middle Jurassic, probably related to relief development. In the Fergana Basin, large conglomerate packages were deposited at the Jurassic-Cretaceous transition, which are traceable around the whole Tien Shan. In the conglomerate of the Tash-Komyr section, a mafic sill with an emplacement age of  $144 \pm 8$  Ma (apatite U-Pb LA-

ICP-MS) indicates small-scale volcanism during the Early Cretaceous. The lack of organic-rich sediments, together with the presence of abundant calcareous paleosols in the Tash-Komyr section, indicates a climate change to (semi-)arid conditions. In the studied basins east of the TFF, no Upper Jurassic – Cretaceous sediment is deposited or preserved.

c) During the Late Cretaceous - early Paleogene, the sediments west of the TFF represent alluvial plain and shallow lake deposits with some marine incursions from the west related to the proto-Paratethys Sea. The dominance of Caledonian (ca 470-390 Ma) ages in the lower Paleogene detrital samples indicates a change in topography whereby the drainage areas became larger towards the NTS - MTS to the east of the TFF where low-relief land area was maintained and where large Caledonian plutons are more prominent compared to scattered Pennsylvanian - Permian granitoids. East of the TFF, sedimentation locally resumed during the early Paleogene with the deposition of continental red beds.

### **Acknowledgements**

This research was supported by the DARIUS program. F. I. Zhimulev's contribution was supported by state assignment project N 0330-2016-0015 and S. Glorie's contribution was supported by ARC DP150101730 and forms TRaX record 380. We want to thank C. Ormukov, E. Bataleva, E. Senchenko and S. Jolivet for their help during the field expeditions. We are also very grateful to A.-E. Debeer for her assistance in our laboratory in Ghent, to M. Dumon for his help with QGIS, to I. Bandurak for his advice regarding the geology of Kyrgyzstan and to A. Käßner and L. Ratschbacher for the use of the zircon U-Pb database of Käßner et al. (2016), GSA Data Repository item 2016247. Reviews of the original manuscript by Dr. D. Alexeiev, Dr. D. Konopelko, Dr. D. Song and two anonymous reviewers were very helpful and contributed to this final version of the paper. We sincerely thank the Gondwana Research

team and especially Dr. I. Safonova for the efficient editorial work. This paper is dedicated to our lovely friend and colleague Vlad Batalev who passed away in August 2017, far too early.

ACCEPTED MANUSCRIPT

## References

Abdrakhmatov, K. Ye., Aldazhanov, S.A., Hager, B.H., Hamburger, M.W., Herring, T.A., Kalabaev, K.B., Makarov, V.I., Molnar, P., Panasyuk, S.V., Prilepin, M.T., Reilinger, R.E., Sadybakasov, I.S., Souter, B.J., Trapeznikov, Yu. A., Tsurkov, V. Ye., Zubovich, A.V. (1996). Relatively recent construction of the Tien Shan inferred from GPS measurements of present-day crustal deformation. *Nature*, 384, 450-453.

Abdrakhmatov, K., Weldon, R., Thompson, S., Burbank, D., Rubin, C., Miller, M., Molnar, P. (2001). Onset, style and current rate of shortening in the central Tien Shan, Kyrgyz Republic. *Russian Geology and Geophysics*, 42 (10), 1585-1609.

Alekseev, D. V., Degtyarev, K.E., Kotov, A. B., Sal'nikova, E. B., Tret'yakov, A. A., Yakovleva, S. Z., Anisimova, I. V., Shatagin, K. N. (2009). Late Paleozoic Subductional and Collisional Igneous Complexes in the Naryn Segment of the Middle Tien Shan (Kyrgyzstan). *Doklady Earth Sciences*, 427 (5), 760-763.

Alexeiev, D.V., Ryazantsev, A.V., Kröner, A., Tret'yakov, A. A., Xia, X., Liu, D.Y. (2011). Geochemical data and zircon ages for rocks in a high-pressure belt of Chu-Yili Mountains, southern Kazakhstan: Implications for the earliest stages of accretion in Kazakhstan and the Tianshan. *Journal of Asian Earth Sciences*, 42, 805-820.

Alexeiev, D. V., Cook, H. E., Djenchuraeva, A. V., Mikolaichuk, A. V. (2015). The stratigraphic, sedimentological and structural evolution of the southern margin of the Kazakhstan

continent in the Tien Shan Range during the Devonian to Permian. In: Brunet, M.F., McCann, T. Sobel, E. R. (Eds.), *Geological Evolution of Central Asian Basins and the Western Tien Shan Range*. Geological Society, London, Special Publications, 427, doi: 10.1144/SP427.3

Alexeiev, D. V., Kröner, A., Hegner, E., Rojas-Agramonte, Y., Biske, Y. S., Wong, J., Geng, H.Y., Ivleva, E.A., Mühlberg, M., Mikolaichuk, A.V., Liu, D. (2016). Middle to Late Ordovician arc system in the Kyrgyz Middle Tianshan: From arc-continent collision to subsequent evolution of a Palaeozoic continental margin. *Gondwana Research*, 39, 261-291.

Alexeiev, D.V., Bykadorov, V.A., Volozh, Yu.A., Sapozhnikov, R.B. (2017). Kinematic analysis of Jurassic grabens of Southern Turgai and the role of the Mesozoic stage in the evolution of the Karatau–Talas–Ferghana strike-slip fault, Southern Kazakhstan and Tian Shan. *Geotectonics*, 51(2), 105–120. doi: 10.1134/S0016852117020029

Aliiev M. M., Genkina R. Z., Dubrovskaya E. N., Nikishova V. M. (1981). Jurassic continental deposits of the east Middle Asia (data, dismemberment, correlation), Moscow, Nauka, 188 p. (in Russian)

Allen, M.B., Windley, B.F., Chi, Z., Zhong-Yan, Z., Guang-Rei, W. (1991). Basin evolution within and adjacent to the Tien Shan Range, NW China. *Journal of Geological Society*, London, 148, 369-378.

Allen, M.B., Alsop, G.I., Zhemchuzhnikov, V.G. (2001). Dome and basin refolding and transpressive inversion along the Karatau fault System, southern Kazakstan. *Journal of the Geological Society of London*, 158, 83–95.

Angiolini, L., Zanchi, A., Zanchetta, S., Nicora, A., Vezzoli, G. (2013). The Cimmerian geopuzzle: New data from South Pamir, *Terra Nova*, 25, 352-360.

Arnaud, N. O., Brunel, M., Cantagrel, J. M., Tapponnier, P. (1993). High cooling and denudation rates at Kongur Shan, Eastern Pamir (Xinjiang, China) revealed by  $^{40}\text{Ar}/^{39}\text{Ar}$  alkali feldspar thermochronology. *Tectonics*, 12(6), 1335-1346.

Bachmanov, D. M., Trifonov, V. G., Mikolaichuk, A. V., Vishnyakov, F. A., & Zarshchikov, A. A. (2008). The Ming-Kush-Kökömeren zone of recent transpression in the Middle Tien Shan. *Geotectonics*, 42(3), 186-205.

Bande, A., Radjabov, S., Sobel, E. R., Sim, T. (2015a). Cenozoic palaeoenvironmental and tectonic controls on the evolution of the northern Fergana Basin. Geological Society, London, Special Publications, 427, <http://doi.org/10.1144/SP427.12>.

Bande, A., Sobel, E. R., Mikolaichuk, A., Torres Acosta, V. (2015b). Talas-Fergana Fault Cenozoic timing of deformation and its relation to Pamir indentation. In: Brunet, M.F., McCann, T. Sobel, E. R. (Eds.), *Geological Evolution of Central Asian basins and the Western Tien Shan Range*. Geological Society, London, Special Publications, 427, doi: 10.1144/SP427.1.

Bazhenov, M. L., Burtman, V. S., Dvorova, A. V. (1999). Permian paleomagnetism of the Tien Shan fold belt, Central Asia: post-collisional rotations and deformation. *Tectonophysics*, 312, 303-329.

Bebeshev, I. I. (1995). Jurassic sedimentary basins in the Central Asian Orogenic Belt. *Lithology and Mineral Resources*, 3, 252-272.

Belgovskiy G. L., Ektova L. A., Maslova E. V. (1958). Explanation note to the sheet K-43-XXXIII of the Geological map of USSR, scale 1:200 000, 106 p. (in Russian).

Bershaw, J., Garzzone, C. N., Schoenbohm, L., Gehrels, G., Tao, L. (2012). Cenozoic evolution of the Pamir plateau based on stratigraphy, zircon provenance, and stable isotopes of foreland basin sediments at Oyttag (Wuyitake) in the Tarim Basin (west China). *Journal of Asian Earth Sciences*, 44, 136-148.

Birkeland P.W. (1974). *Pedology, Weathering, and Geomorphological Research*. Oxford University Press, New York, N.Y., 285 p.

Biske G. S., Zubtsov S. E. (1985). Geology map of USSR, sheet K 43-XXXII, scale 1:200 000, Alay-Kokshal series.

Biske, Yu. S., Seltmann, R. (2010). Paleozoic Tian-Shan as a transitional region between the Rheic and Urals-Turkestan oceans. *Gondwana Research*, 17, 602-613.

Biske, Y. S., Konopelko, D. L., Seltmann, R. (2013). Geodynamics of Late Paleozoic Magmatism in the Tien Shan and Its Framework. *Geotectonics*, 47, 291-309.

Blair, T. C., McPherson, J. G. (1994). Alluvial fans and their natural distinction from rivers based on morphology, hydraulic processes, sedimentary processes and facies assemblages. *Journal of Sedimentary Research*, A64, 450–489.

Blair, T. C. (1999). Sedimentology of the debris-flow- dominated Warm Spring Canyon alluvial fan, Death Valley, California. *Sedimentology*, 46, 941–965.

Bosboom, R. E., Dupont-Nivet, G., Houben, A. J. P., Brinkhuis, H., Villa, G., Mandic, O., Stoica, M., Zachariasse, W. J., Guo, Z., Li, C., Krijgsman, W. (2011). Late Eocene sea retreat from the Tarim Basin (west China) and concomitant Asian paleoenvironmental change. *Palaeogeography, Palaeoclimatology, Palaeoecology*, 299, 385-398.

Bosboom, R., Dupont-Nivet, G., Grothe, A., Brinkhuis, H., Villa, G., Mandic, O., Stoica, M., Kouwenhoven, T., Huang, W., Yang, W., Guo, Z. (2014). Timing, cause and impact of the late Eocene stepwise sea retreat from the Tarim Basin (west China). *Palaeogeography, Palaeoclimatology, Palaeoecology*, 403, 101-118.

Bosboom, R., Mandic, O., Dupont-Nivet, G., Proust, J-N., Ormukov, C., Aminov, J. (2015). Late Eocene palaeogeography of the proto-Paratethys Sea in Central Asia (NW China, southern Kyrgyzstan and SW Tajikistan). In: Brunet, M.F., McCann, T. Sobel, E. R. (Eds.), *Geological*

Evolution of Central Asian Basins and the Western Tien Shan Range. Geological Society, London, Special Publications, 427, doi: 10.1144/SP427.3, <http://doi.org/10.1144/SP427.11>

Bougeois, L., de Rafélis, M., de Nooijer, L, Reichart, G.-J., Nicollin, F., Dupont-Nivet, G. (2014). A high resolution study of trace elements and stable isotopes in oyster shells to estimate Central Asian Middle Eocene seasonality. *Chemical Geology*, 363, 200–212.

Brookfield, M. E. (2000). Geological development and Phanerozoic crustal accretion in the western segment of the southern Tien Shan (Kyrgyzstan, Uzbekistan and Tajikistan). *Tectonophysics*, 328, 1-14.

Bullen, M.E., Burbank, D.W., Garver, J.I., Abdrakhmatov, K. Ye. (2001). Late Cenozoic tectonic evolution of the northwestern Tien Shan: New age estimates for the initiation of mountain building. *Geological Society of America Bulletin*, 113 (12), 1544-1559.

Bullen, M. E., Burbank, D. W., Garver, J. I. (2003). Building the Northern Tien Shan: Integrated thermal, structural, and topographic constraints. *Journal of Geology*, 111(2), 149-165.

Burbank, D.W., McLean, J.K., Bullen, M., Abdrakhmatov, K.Y., Miller, M.M. (1999). Partitioning of intermontane basins by thrust-related folding, Tien Shan, Kyrgyzstan. *Basin Research*, 11, 75-92.

Burtman, V. S. (1964). Talas-Fergana Fault (Tien Shan), Geological Institute Academy of Sciences USSR, Transactions, 104, Moscow, Nauka, 143p. (in Russian).

Burtman, V. S., Skobelev, S. F., Molnar, P. (1996). Late Cenozoic slip on the Talas-Ferghana fault, the Tien Shan, central Asia. Geological Society of America Bulletin, 108 (8), 1004-1021.

Burtman, V. S. (2000). Cenozoic crustal shortening between the Pamir and Tien Shan and a reconstruction of the Pamir-Tien Shan transition zone for the Cretaceous and Paleogene. Tectonophysics, 319, 69-92.

Burtman, V.S. (2010). Tien Shan, Pamir, and Tibet: History and Geodynamics of Phanerozoic Oceanic Basins. Geotectonics, 44 (5), 388-404.

Burtman, V. S. (2012). Geodynamics of Tibet, Tarim, and the Tien Shan in the Late Cenozoic (2012). Geotectonics, 46, 185-211.

Burtman, V. S. (2015). Tectonics and Geodynamics of the Tian Shan in the Middle and Late Paleozoic. Geotectonics, 49 (4), 302-319.

Buvalkin, A.K., Jaimin, M.I., Kotova, L.I., Philip'ev, G.P. (1991). The Preichim–Karatau area during the early Jurassic and its coal-bearing and oil and gas capacity perspectives. In: Shlygin, A.E. (ed.) Geological Structure and Mineralogy of South Kazakhstan, Gulyym, Alma-Ata, Kazakhstan, 110–128 (in Russian).

Carroll, A. R., Dumitru, T. A., Graham, S. A., Hendrix, M. S. (2013). An 800 million-year detrital zircon record of continental amalgamation: Tarim Basin, NW China, *International Geology Review*, 55 (7), 818-829.

Charreau, J., Gilder, S., Chen, Y., Dominguez, S., Avouac, J-Ph, Sen, S., Jolivet, M., Li, Y., Wang, W.M. (2006). Magnetostratigraphy of the Yaha section, Tarim Basin (China): 11 Ma acceleration in erosion and uplift of the Tian Shan mountains. *Geology*, 34 (3), 181-184.

Chen, X., Wang, Z., Chen, Z., Seitmuratova, E., Han, S., Zhou, Q., Ye, B. (2015). SHRIMP U–Pb, Ar–Ar and fission-track geochronology of W–Mo deposits in the Balkhash Metallogenic Belt (Kazakhstan), Central Asia, and the geological implications. *Journal of Asian Earth Sciences*, 110, 19-32.

Choulet, F., Chen, Y., Cogné, J. P., Rabillard, A., Wang, B., Lin, W., Faure, M., Cluzel, D. (2013). First Triassic palaeomagnetic constraints from Junggar (NW China) and their implications for the Mesozoic tectonics in Central Asia. *Journal of Asian Earth Sciences*, 78, 371-394.

Clarke, J.W. (1984). Geology and possible uranium deposits of the Fergana region of Soviet Central Asia: United States Geological Survey Open-File Report 84-513.

Cobbold, P.R., Sadybakasov, E., Thomas, J.C. (1994). Cenozoic transpression and basin development, Kyrgyz Tianshan, Central Asia. In: Roure, F., Ellouz, N., Shein, V.S., Skvortsov, I. (Eds.), *Geodynamic Evolution of Sedimentary Basins*. International Symposium, Moscow, 181–202.

Corfu, F., Hanchar, J.M., Hoskin, P.W.O., Kinny, P. (2003). Atlas of zircon textures. *Reviews in Mineralogy and Geochemistry*, 53, 469–500.

Coutand, I., Strecker, M. R., Arrowsmith, J. R., Hilley, G., Thiede, R. C., Korjenkov, A., Omuraliev, M. (2002). Late Cenozoic tectonic development of the intramontane Alai Valley, (Pamir-Tien Shan region, central Asia): An example of intracontinental deformation due to the Indo-Eurasia collision. *Tectonics*, 21 (6), 1053.

De Grave, J., Buslov, M.M., Van den haute, P. (2007). Distant effects of India-Eurasia convergence and Mesozoic intracontinental deformation in Central Asia: Constraints from apatite fission-track thermochronology. *Journal of Asian Earth Sciences*, 29, 188-204.

De Grave, J., Van den haute, P., Buslov, M. M., Dehandschutter, B., Glorie, S. (2008). Apatite fission-track thermochronology applied to the Chulyshman Plateau, Siberian Altai Region. *Radiation Measurements*, 43, 38-42.

De Grave, J., Buslov, M.M., Van den haute, P., Metcalf, J., Dehandschutter, B., McWilliams, M.O. (2009). Multi-method chronometry of the Teletskoye graben and its basement, Siberian Altai Mountains: new insights on its thermo-tectonic evolution. From: Lisker, F., Ventura, B., Glasmacher, U.A. *Thermochronological methods: From paleotemperature Constraints to Landscape evolution models*. Geological Society, London, Special Publications, 324, 237-259.

De Grave, J., Glorie, S., Buslov, M.M., Izmer, A., Fournier-Carrie, A., Elburg, M., Batalev, V. Yu., Vanhaeke, F., Van den haute, P. (2011). The thermo-tectonic history of the Song-Kul Plateau, Kyrgyz Tien Shan: constraints by apatite and titanite thermo-chronometry and zircon U-Pb dating. *Gondwana Research*, 20, 745-763.

De Grave, J., Glorie, S., Ryabinin, A., Zhimulev, F. Izmer, A., Buslov, M.M., Elburg, M., Vanhaeke, F., Van den haute, P. (2012). Late Palaeozoic and Meso-Cenozoic tectonic evolution of the Southern Kyrgyz Tien Shan: constraints from multi-method thermochronology in the Trans-Alai, Turkestan-Alai Section and the Southeastern Ferghana Basin. *Journal of Asian Earth Sciences*, 44, 149-168.

De Grave, J. , Glorie, S., Buslov, M.M., Stockli, D.F., McWilliams, M.O., Batalev, V. Y., Van den haute P. (2013). Thermo-tectonic history of the Issyk-Kul basement (Kyrgyz Northern Tien Shan, Central Asia). *Gondwana Research*, 23, 998-1020.

Degtyarev, K. E. (2011). Tectonic evolution of Early Paleozoic island-arc systems and continental crust formation in the Caledonides of Kazakhstan and the North Tien Shan. *Geotectonics*, 45 (1), 23-50.

Delvaux, D., Cloetingh, S., Beekman, F., Sokoutis, D., Burov, E., Buslov, M.M., Abdrakhmatov, K.E. (2013). Basin evolution in a folding lithosphere: Altai-Sayan and Tien Shan belts in Central Asia. *Tectonophysics*, 602, 194-222.

De Pelsmaeker, E., Glorie, S., Buslov, M. M., Zhimulev, F., Poujol, M., Korobkin, V. V., Vanhaecke, F., Vetrov, E. V., De Grave, J. (2015). Late-Paleozoic emplacement and Mesozoic reactivation of the southern Kazakhstan granitoid basement. *Tectonophysics*, 662, 416-433.

Dercourt, J., Ricou, L.E., Vrielynck, B. (1993). Atlas Tethys Paleoenvironmental Maps. Commission for the Geological Map of the World, Paris, p. 269.

Dolgoplova, A., Seltmann, R., Konopelko, D., Biske, Yu. S., Shatov, V., Armstrong, R., Belousova, E., Pankhurst, R., Koneev, R., Divaev, F. (2017). Geodynamic evolution of the western Tien Shan, Uzbekistan: Insights from U-Pb SHRIMP geochronology and Sr-Nd-Pb-Hf isotope mapping of granitoids. *Gondwana Research*, 47, 76-109.

Ducea, M. N., Lutkov, V., Minaev, V. T., Hacker, B., Ratschbacher, L., Luffi, P., Schwab, M., Gehrels, G. E., McWilliams, M., Vervoort, J., Metcalf, J. (2003). Building the Pamirs: The view from the underside. *Geology*, 31, 849-852.

Dumitru, T.A., Zhou, D., Chang, E.Z., Graham, S.A., Hendrix, M. S., Sobel, E. R., Carroll, A. R. (2001). Uplift, exhumation, and deformation in the Chinese Tian Shan. In: Hendrix, M. S., and Davis, G. A. (Eds), *Paleozoic and Mesozoic tectonic evolution of central and eastern Asia: From continental assembly to intracontinental deformation*. Geological Society of America Memoir 194, p. 71-99.

Eberth, D.A., Brinkman, D.B., Chen, P.-J., Yuan, F.-T., Wu, S.-Z., Li, G., Cheng, X.-S. (2001). Sequence stratigraphy, paleoclimate patterns, and vertebrate fossil preservation in Jurassic-Cretaceous strata of the Junggar Basin, Xinjiang Autonomous Region, People's Republic of China. *Canadian Journal of Earth Sciences*, 38(12), 1627-1644.

Fang, Y., Wu, C., Guo, Z., Hou, K., Dong, L., Wang, L., Li, L. (2015). Provenance of the southern Junggar Basin in the Jurassic: Evidence from detrital zircon geochronology and depositional environments. *Sedimentary Geology*, 315, 47-63.

Feld, C., Haberland, C., Schurr, B., Sippl, C., Wetzel, H.-A., Roessner, S., Ickrath, M., Abdybachaev, U., Orunbaev, S. (2015). Seismotectonic study of the Fergana Region (Southern Kyrgyzstan): distribution and kinematics of local seismicity. *Earth, Planets and Space*, 67, 1-13.

Fraser, J. E., Searle, M. P., Parrish, R. R., Noble, S. R. (2001). Chronology of deformation, metamorphism, and magmatism in the southern Karakoram Mountain, *Geological Society of America Bulletin*, 113, 1443-1455.

Genkina, R. Z. (1977). Stratigraphy of Jurassic continental rocks of the Fergana Range and paleobotanic substantiation of their age. *Sovetskaya Geologia*, 9, 61-79. (In Russian).

Gillespie, J., Glorie, S., Xiao, W., Zhang, Z., Collins, A. S., Evans, N., McInnes, B., De Grave, J. (2017). Mesozoic reactivation of the Beishan, southern Central Asian Orogenic Belt: Insights from low-temperature thermochronology, *Gondwana Research*, 43, 107-122.

Glorie, S., De Grave, J., Buslov, M.M., Elburg, M.A., Stockli, D.F., Gerdes, A., Van den haute, P. (2010). Multi-method chronometric constraints on the evolution of the Northern Kyrgyz Tien Shan granitoids (Central Asian Orogenic Belt): From emplacement to exhumation. *Journal of Asian Earth Sciences*, 38, 131-146.

Glorie, S., De Grave, J., Buslov, M.M., Zhimulev, F.I., Stockli, D.F., Batalev, V.Yu., Izmer, A., Van den haute, P., Vanhaecke, F., Elburg, M.A. (2011). Thermotectonic history of the Kyrgyz South Tien Shan (Atbashi-Inylchek) suture zone: the role of inherited structures during deformation-propagation. *Tectonics*, 30, TC6016.

Glorie, S., De Grave, J., Buslov, M.M., Zhimulev, F.I., Elburg, M.A., Van den haute, P. (2012). Structural control on Meso-Cenozoic tectonic reactivation and denudation in the Siberian Altai: Insights from multi-method thermochronometry. *Tectonophysics*, 544-545, 75-92.

Glorie, S. and De Grave, J. (2016). Exhuming the Meso-Cenozoic Kyrgyz Tianshan and Siberian Altai-Sayan: A review based on low-temperature thermochronology. *Geoscience Frontiers*, 7, 155-170.

Goode, J.K., Burbank, D.W., Ormukov, C. (2014). Pliocene-Pleistocene initiation, style, and sequencing of deformation in the central Tien Shan. *Tectonics*, 33, 464-484.

Graham, S.A., Brassell, S., Carroll, A.R., Xiao, X., Demaison, G., McKnight, C.L., Liang, Y., Chu, J., Hendrix, M.S. (1990). Characteristics of selected petroleum source rocks, Xianjiang Uygur

autonomous region, Northwest China. *American Association of Petroleum Geologists Bulletin*, 74(4), 493-512.

Grewingk, C. (1853). Die geognostischen und orographischen Verhaeltnisse des noerdlichen Persiens. *Verhandlungen der R.K Mineralogischen Gesellschaft*, 1852–1853, 97–245.

Han, B.F., Ji, J.Q., Song, B., Chen, L.H., Zhang, L. (2006). Late Paleozoic vertical growth of continental crust around the Junggar Basin, Xinjiang, China (Part I): Timing of post-collisional plutonism. *Acta Petrologica Sinica*, 22, 1077-1086.

Han, Y., Zhao, G., Sun, M., Eizenhöfer, P.R., Hou, W., Zhang, X., Liu, D., Wang, B., Zhang, G. (2015). Paleozoic accretionary orogenesis in the Paleo-Asian Ocean: Insights from detrital zircons from Silurian to Carboniferous strata at the northwestern margin of the Tarim Craton. *Tectonics*, 34, 334-351, doi:10.1002/2014TC003668.

Han, Y., Zhao, G., Sun, M., Eizenhöfer, P.R., Hou, W., Zhang, X., Liu, D., Wang, B. (2016). Detrital zircon provenance constraints on the initial uplift and denudation of the Chinese western Tianshan after the assembly of the southwestern Central Asian Orogenic Belt. *Sedimentary Geology*, 339, 1-12.

Hasiotis, S. T., Kraus, M. J., Demko, T. M. (2007). Climatic controls on continental trace fossils. In: Miller, W. III (Ed.) *Trace Fossils: Concepts, Problems, Prospects*. Elsevier, Amsterdam, 172–195.

Heermance, R.V., Chen, J., Burbank, D.W., Miao, J. (2008). Temporal constraints and pulsed Late Cenozoic deformation during the structural disruption of the active Kashi foreland, northwest China. *Tectonics*, 27, TC6012, doi:10.1029/2007TC002226.

Hegner, E., Klemm, R., Kröner, A., Corsini, M., Alexeiev, D.V., Iaccheri, L.M., Zack, T., Dulski, P., Xia, X., Windley, B.F. (2010). Mineral ages and P-T conditions of Late Paleozoic High-Pressure eclogite and provenance of mélangé sediments from Atbashi in the Southern Tianshan Orogen of Kyrgyzstan. *American Journal of Science*, 310, 916-950.

Hendrix, M. S., Graham, S. A., Carroll, A. R., Sobel, E. R., McKnight, C. L., Schulein, B. J., Wang, Z. (1992). Sedimentary record and climatic implications of recurrent deformation in the Tien Shan: Evidence from Mesozoic strata of the north Tarim, south Junggar, and Turpan basins, Northwest China. *Geological Society of America Bulletin*, 104 (1), 53-79.

Hendrix, M. S. (2000). Evolution of Mesozoic sandstone compositions, southern Junggar, northern Tarim and western Turpan basins, northwest China: A detrital record of the ancestral Tian Shan. *Journal of Sedimentary Research*, 70(3), 520-532.

Heng-Ren, Y., Tian-Fu, T., Xiu, L., Lan-Ying, H., Cong-Liu, Y., Yi-Yong, Z., Shi-Lan, Z., Jing-Ming, W. (1983). A preliminary study of the Upper Cretaceous of the Western Tarim Basin (South Xinjiang, China) with special reference to its transgressions. *Zitteliana*, 10, 115-121.

Hjulström, F. (1952). The geomorphology of the alluvial outwash plains (Sandurs) of Iceland, and the mechanics of braided rivers. Proceedings of the 17th International Congress of the International Geographical Union, Washington, 337-342.

Hoskin, P. W. O., Black, L. P. (2000). Metamorphic zircon formation by solid-state recrystallization of protolith igneous zircon. *Journal of Metamorphic Geology*, 18 (4), 423-439.

Hoskin, P. W. O., Ireland, T. R. (2000). Rare earth element chemistry of zircon and its use as a provenance indicator. *Geology*, 28 (7), 627-630.

Hoskin, P.W.O., Schaltegger, Urs. (2003). The composition of Zircon and Igneous and Metamorphic Petrogenesis. *Reviews in Mineralogy and Geochemistry*, 53 (1), 27-62.

Jackson, S.E., Pearson, N.J., Griffin, W.L., Belousova, E. (2004). The application of laser ablation inductively coupled plasma mass spectrometry to in-situ U-Pb zircon geochronology. *Chemical Geology*, 211, 47-69.

Jia, Y., Fu, B., Jolivet, M., Zheng, Sh. (2015). Cenozoic tectono-geomorphological growth of the SW Chinese Tian Shan : Insight from AFT and detrital zircon U-Pb data. *Journal of Asian Earth Sciences*, 111, 395-413.

Jolivet, M., Ritz, J.-F., Vassallo, R., Larroque, C., Braucher, R., Todbileg, M., Chauvet, A., Sue, C., Arnaud, N., De Vicente, R., Arzhanikova, A., Arzhanikov, S. (2007). The Mongolian

summits: An uplifted, flat, old but still preserved erosion surface. *Geology*, 35 (10), 871-874.

doi: 10.1130/G23758A.1

Jolivet, M., Dominguez, S., Charreau, J., Chen, Y., Li, Y. G., Wang, Q. C. (2010). Mesozoic and Cenozoic tectonic history of the central Chinese Tian Shan: reactivated tectonic structures and active deformation. *Tectonics*, 29, TC6019.

Jolivet, M., Arzhannikov, S., Arzhannikova, A., Chauvet, A., Vassallo, R., Braucher, R. (2013a). Geomorphic Mesozoic and Cenozoic evolution in the Oka-Jombolok region (East Sayan ranges, Siberia). *Journal of Asian Earth Sciences*, 62, 117-132.

Jolivet, M., Heilbronn, G., Robin, C., Barrier, L., Bourquin, S., Guo, Zh., Jia, Y., Guerit, L., Yang, W., Fu, B. (2013b). Reconstructing the Late Palaeozoic – Mesozoic topographic evolution of the Chinese Tian Shan: available data and remaining uncertainties. *Advances in Geosciences*, 1, 1-12.

Jolivet, M. (2015). Mesozoic tectonic and topographic evolution of Central Asia and Tibet: a preliminary synthesis. In: Brunet, M.F., McCann, T. Sobel, E. R. (Eds.), *Geological Evolution of Central Asian Basins and the Western Tien Shan Range*. Geological Society, London, Special Publications, 427, doi: 10.1144/SP427.

Jolivet, M., Bourquin, S., Heilbronn, G., Robin, C., Barrier, C., Dabard, M.-P., Jia, Y., De Pelsmaeker, E., Fu, B. (2015). The Upper Jurassic–Lower Cretaceous alluvial-fan deposits of the Kalaza Formation (Central Asia): tectonic pulse or increased aridity? In: Brunet, M.F.,

McCann, T. Sobel, E. R. (Eds.), Geological Evolution of Central Asian Basins and the Western Tien Shan Range. Geological Society, London, Special Publications, 427, doi:10.1144/SP427.6.

Jolivet, M., Arzhannikova, N., Frolov, A. O., Arzhannikov, S., Kulagina, N., Akulova, V., Vassallo, R. (2017). Late Jurassic–Early Cretaceous paleoenvironment evolution of the Transbaikalian basins (SE Siberia): Implications for the Mongol–Okhotsk orogeny. *Bulletin Société Géologique de France*, 188(1-2), 101-118.

Käßner, A., Ratschbacher, L., Pfänder, J.A., Hacker, B.R., Zack, G., Sonntag, B.-L., Khan, J., Stanek K.P., Gadoev, M. and Oimahmadov, I. (2016). Proterozoic–Mesozoic history of the Central Asian orogenic belt in the Tajik and southwestern Kyrgyz Tian Shan: U–Pb,  $^{40}\text{Ar}/^{39}\text{Ar}$ , and fission-track geochronology and geochemistry of granitoids. *The Geological Society of America Bulletin*, 129 (3-4), 281-303. doi: 10.1130/B31466.1

Konopelko, D., Biske, G., Seltmann, R., Eklund, O., Belyatsky, B. (2007). Hercynian post-collisional A-type granites of the Kokshaal Range, southern Tien Shan, Kyrgyzstan. *Lithos*, 97(1), 140-160.

Konopelko, D., Biske, G., Seltmann, R., Kiseleva, M., Matukov, D., Sergeev, S. (2008). Deciphering Caledonian events: timing and geochemistry of the Caledonian magmatic arc in the Kyrgyz Tien Shan. *Journal of Asian Earth Sciences*, 32(2), 131-141.

Konopelko, D., Seltmann, R., Biske, G., Lepekhina, E., Sergeev, S. (2009). Possible source dichotomy of contemporaneous post-collisional barren I-type versus tin-bearing A-type

granites, lying on opposite sides of the South Tien Shan suture. *Ore Geology Reviews*, 35(2), 206-216.

Konopelko, D., Kullerud, K., Apayarov, F., Sakiev, K., Baruleva, O., Ravna, E., Lepekhina, E. (2012). SHRIMP zircon chronology of HP-UHP rocks of the Makbal metamorphic complex in the Northern Tien Shan, Kyrgyzstan. *Gondwana Research*, 22(1), 300-309.

Konopelko, D., Seltmann, R., Apayarov, F., Belousova, E., Izokh, A., Lepekhina, E. (2013). U–Pb–Hf zircon study of two mylonitic granite complexes in the Talas-Fergana fault zone, Kyrgyzstan, and Ar–Ar age of deformations along the fault. *Journal of Asian Earth Sciences*, 73, 334-346.

Konopelko, D., Biske, G., Seltmann, R., Petrov, S. V., Lepekhina, E. (2014). Age and petrogenesis of the Neoproterozoic Chon-Ashu alkaline complex, and a new discovery of chalcopyrite mineralization in the eastern Kyrgyz Tien Shan. *Ore Geology Reviews*, 61, 175-191.

Konopelko, D., Klemd, R., Mamadjanov, Y., Hegner, E., Knorsch, M., Fidaev, D., Kern, M., Sergeev, S. (2015). Permian age of orogenic thickening and crustal melting in the Garm Block, South Tien Shan, Tajikistan. *Journal of Asian Earth Sciences*, 113, 711-727.

Konopelko, D., Klemd, R. (2016). Deciphering protoliths of the (U)HP rocks in the Makbal metamorphic complex, Kyrgyzstan: geochemistry and SHRIMP zircon geochronology. *European Journal of Mineralogy*, 28, 1233-1253.

Konopelko, D., Klemd, R., Petrov, S. V., Apayarov, F., Nazaraliev, B., Vokueva, O., Scherstén, A., Sergeev, S (2017a). Precambrian gold mineralization at Djamgyr in the Kyrgyz Tien Shan: tectonic and metallogenic implications. *Ore Geology Reviews*, 86, 537–547.

Konopelko, D., Seltmann, R., Mamadjanov, Y., Romer, R. L., Rojas-Agramonte, Y., Jeffries, T., Fidaev, D., Niyozov, A. (2017b). A geotraverse across two paleo-subduction zones in Tien Shan, Tajikistan. *Gondwana Research*, 47, 110-130.

Korzhenkov, A.M., Rogozhin, E.A., Xuhui, s., Qinjian, T., Yueren, X. (2014). Strong paleoearthquakes along the Talas-Fergana Fault, Kyrgyzstan. *Geodesy and Geodynamics*, 5 (1), 11-19.

Kuzichkina, Yu. M. (1972). Jurassic system. In: Pomazkov, K. D. (Ed.), *Geology of the USSR*, v25, *Geology of Kyrgyz SSR*, Nedra, Moscow, pp. 208–224. (In Russian)

Kröner, A., Hegner, E., Lehmann, B., Heinhorst, J., Wingate, M.T.D., Liu, D.Y., Ermelov, P. (2008). Palaeozoic arc magmatism in the Central Asian Orogenic Belt of Kazakhstan: SHRIMP zircon ages and whole-rock Nd isotopic systematics. *Journal of Asian Earth Sciences*, 32, 118–130.

Kröner, A., Alexeiev, D. V., Hegner, E., Rojas-Agramonte, Y., Corsini, M., Chao, Y., Wong, J., Windley, B.F., Liu, D. Tretyakov, A. A. (2012). Zircon and muscovite ages, geochemistry, and

Nd–Hf isotopes for the Aktyuz metamorphic terrane: evidence for an Early Ordovician collisional belt in the northern Tianshan of Kyrgyzstan. *Gondwana Research*, 21 (4), 901-927.

Kröner, A., Alexeiev, D. V., Rojas-Agramonte, Y., Hegner, E., Wong, J., Xia, X., Belousova, E., Mikolaichuk, A.V., Seltmann, R., Liu, D., Kiselev, V. V. (2013). Mesoproterozoic (Grenville-age) terranes in the Kyrgyz North Tianshan: zircon ages and Nd–Hf isotopic constraints on the origin and evolution of basement blocks in the southern Central Asian Orogen. *Gondwana Research*, 23 (1), 272-295.

Kröner, A., Alexeiev, D.V., Kovach, V.P., Rojas-Agramonte, Y., Tretyakov, A.A., Mikolaichuk, A.V., Xie, H., Sobel, E.R. (2017). Zircon ages, geochemistry and Nd isotopic systematics for the Palaeoproterozoic 2.3-1.8 Ga Kuilyu Complex, East Kyrgyzstan – The oldest continental basement fragment in the Tianshan orogenic belt. *Journal of Asian Earth Sciences*, 135, 122-135.

Lan, X. (1997). Paleogene bivalve communities in the western Tarim Basin and their paleoenvironmental implications. *Paleoworld* 7, 137–157.

Lasovskiy A. G., Mozolev L. N. (1961). Geology map of USSR, sheet K 43-XXI, scale 1:200 000, Northern Tian-Shan series.

Lee, K. Y. (1985). Geology of the Tarim Basin with special emphasis on petroleum deposits, Xinjiang Uygur Zizhiqu, Northwest China. U.S. Geological Survey Reston, Virginia. Open-File Rep., 85- 616, 55 pp.

Li, Z., Song, W., Peng, S., Wang, D., Zhang, Z. (2004). Meso-Cenozoic tectonic relationships between the Kuqa subbasin and Tian Shan, northwest China: constraints from depositional records. *Sedimentary Geology*, 172, 223-249.

Li, Z., Peng, S. (2010). Detrital zircon geochronology and its provenance implications: responses to Jurassic through Neogene basin-range interactions along northern margin of the Tarim Basin, Northwest China. *Basin Research*, 22, 126-138.

Li, S. W., Xu, D. K. (2007). Geological map of Chinese Tianshan and adjacent areas, scale 1:1000000. Beijing, Geology Publishing House, 2 sheets. (in Chinese).

Liu, D., Jolivet, M., Yang, W., Zhang, Z., Cheng, F., Zhu, B., Guo Zh. (2013). Latest Palaeozoic – Early Mesozoic basin-range interactions in South Tian Shan (northwest China) and their tectonic significance: Constraints from detrital zircon U-Pb ages. *Tectonophysics*, 599, 197-213.

Liu, D., Guo, Z., Jolivet, M., Cheng, F., Song, Y., Zhang, Z. (2014). Petrology and geochemistry of Early Permian volcanic rocks in South Tian Shan, NW China: Implications for the tectonic evolution and Phanerozoic continental growth. *International Journal of Earth Sciences*, 103, 737 – 756.

Lloyd, J., Collins, A. S., Payne, J. L., Glorie, S., Holford, S., Reid, A. J. (2016). Tracking the Cretaceous transcontinental Ceduna River through Australia: The hafnium isotope record of detrital zircons from offshore southern Australia. *Geoscience Frontiers*, 7, 237-244.

Lomize, M.G. (1996). The Fergana sigmoid and Talas-Fergana strike-slip fault in a collision structure of Central Asia. *Doklady Earth Sciences*, 350, 1100–1103. (in Russian).

Loury, C., Rollan, Y., Cenko-Tok, B., Lanari, P., Guillot, S. (2016). Late Paleozoic evolution of the South Tien Shan: Insights from P-T estimates and allanite geochronology on retrogressed eclogites (Chatkal range, Kyrgyzstan). *Journal of Geodynamics*, 96, 62-80.

Lowe, D. R. (1982). Sediment gravity flows: II. Depositional models with special reference to the deposits of high-density turbidity currents. *Journal of Sedimentary Petrology*, 52(1), 279–297.

Ludwig, K. (2003). User's Manual for Isoplot 3.00, A Geochronological Toolkit for Microsoft Excel. Berkeley Geochronology Center Special Publication v. 4.

Macaulay, E. A., Sobel E. R., Mikolaichuk, A., Kohn, B., Stuart, F. M. (2014). Cenozoic deformation and exhumation history of the Central Kyrgyz Tien Shan. *Tectonics*, 33, 135-165.

Macaulay, E. A., Sobel, E. R., Mikolaichuk, A., Wack, M., Gilder, S. A., Mulch, A., Fortuna, A. B., Hynek, S., Apayarov, F. (2016). The sedimentary record of the Issyk Kul Basin, Kyrgyzstan: climatic and tectonic inferences. *Basin Research*, 28, 57-80, doi: 10.1111/bre.12098.

Mack, G. H., James W. C., Monger, H. C. (1993). Classification of paleosols, Geological Society of America Bulletin, 105, 129-136.

Manzotti, P., Poujol, M., Ballèvre, M. (2015). Detrital zircon geochronology in blueschist-facies meta-conglomerates from the Western Alps: implications for the late Carboniferous to early Permian palaeogeography. International Journal of Earth Sciences, 104, 703-731.

Mather, A. E., Hartley, A. (2005). Flow events on a hyper-arid alluvial fan: Quebrada Tambores, Slar de Atacame, northern Chile. In: Harvey, A. M., Mather, A. E. Stokes, M. (Eds.), Alluvial Fans: Geomorphology, Sedimentology, Dynamics. Geological Society, London, Special Publications, 251, 9–24, <http://doi.org/10.1144/GSL.SP.2005.251.01.02>

McDowell, F.W., McIntosh, W.C., and Farley, K.A. (2005) A precise  $^{40}\text{Ar}$ – $^{39}\text{Ar}$  reference age for the Durango apatite (U–Th)/He and fission-track dating standard. Chemical Geology, 214, 249–263.

McPherson, J. G., Shanmugam, G., Moiola, R. J. (1987). Fan deltas and braid deltas ; varieties of coarse-grained deltas. Bulletin of American Association of Petroleum Geologists, 99, 331-340.

Metelkin, D.V, Vernikovskiy, V.A., Kazansky, A. Y., Wingate, M.T.D. (2010). Late Mesozoic tectonics of Central Asia based on paleomagnetic evidence. Gondwana Research, 18, 400-419.

Miall, A. D. (1996). *The Geology of Fluvial Deposits*. Springer, Berlin, 582 p.

Miall, A. D. (2016). *Stratigraphy : A modern Synthesis*. Springer International Publishing, Switzerland.

Molnar, P., Tapponnier, P. (1975). Cenozoic tectonics of Asia: effects of a continental collision: features of recent continental tectonics in Asia can be interpreted as results of the India-Eurasia collision. *Science*, 189, 419–426.

Morozov, Yu. A., Leonov, M. G., Alekseev, D. V. (2014). Pull-Apart Formation Mechanism of Cenozoic Basins in the Tien Shan and Their Transpressional Evolution: Structural and Experimental Evidence. *Geotectonics*, 48 (1), 24-53.

Mulder, T., Alexander, J. (2001). The physical character of subaqueous sedimentary density flows and their deposits. *Sedimentology*, 48, 269–299.

Nasdala, L., Zhang, M., Kempe, U., Panczer, G., Gaft, M., Andrut, M., Plötze, M. (2003). Spectroscopic methods applied to zircon. In: Hanchar, J. M., Hoskin, P. W. O. (Eds.), *Zircon. Reviews in Mineralogy and Geochemistry*, 53, Mineralogical Society of America, 427–467.

Osmonbetov, K. O., Knauf, V. I., Korolyov, V.T. (Eds.) (1982). *Stratified and Intrusive Formations of Kyrgyzia*, Ilim Publishing House, Frunze, Kyrgyz SSR, Volume 1: 357p; Volume 2: 245 p. (In Russian)

Payne, J. L., Hand, M., Barovich, K. M., Wade, B. P. (2008). Temporal constraints on the timing of high-grade metamorphism in the northern Gawler Craton: implications for assembly of the Australian Proterozoic. *Australian Journal of Earth Sciences*, 55, 623–640.

Pochon, A., Poujol, M., Gloaguen, E., Branquet, Y., Cagnard, F., Gumiaux, C., Gapais, D. (2016). U-Pb LA-ICP-MS dating of apatite in mafic rocks: evidence for a major magmatic event at the Devonian-Carboniferous boundary in the Armorican Massif (France). *American Mineralogist*, 101, 2430–2442.

Postma, G., (1990). Depositional architecture and facies of river and fan deltas : a synthesis. In: Collela, A., Prior, D. B. (Eds.), *Coarse-grained deltas*. International Association of Sedimentologists, Special Publications, 10, 13-27.

Poyarkova, Z. N. (1972). Cretaceous system. In: Pomazkov, K.D. (Ed.), *Geology of the USSR*, v25, *Geology of Kyrgyz SSR*, Nedra, Moscow, pp. 224–236. (In Russian)

Rasskazov, S. V., Chuvashova, I. S., Mikolaichuk, A. V., Sobel, E. R., Yasnygina, T. A., Fefelov, N. N., Saranina, E. V. (2015). Lateral Change of Sources for the Cretaceous–Paleogene Magmatism of the Tian Shan: *Petrology*, 23 (3), 281–308.

Ren, R., Han, B.-F., Ji, J.-Q., Zhang, L., Xu, Z., Su, L. (2011). U–Pb age of detrital zircons from the Tekes River, Xinjiang, China, and implications for tectonomagmatic evolution of the South Tian Shan Orogen. *Gondwana Research*, 19, 460-470.

Retallack, G. J. (1997). *A Colour Guide to Paleosols*. John Wiley and Sons, Chichester, England.

Robinson, A. C., Yin, A., Manning, C. E., Harrison, T. M., Zhang, S. H., Wang, X. F. (2004). Tectonic evolution of the northeastern Pamir: Constraints from the northern portion of the Cenozoic Kongur Shan extensional system, western China, *Geological Society of America Bulletin*, 116, 953-973.

Robinson, A. C. (2015). Mesozoic tectonics of the Gondwana terranes of the Pamir plateau. *Journal of Asian Earth Sciences*, 102, 170-179.

Rolland, Y., Alexeiev, D., Kröner, A., Corsini, M., Loury, C., Monié, P. (2013). Late Palaeozoic to Mesozoic kinematic history of the Talas–Ferghana strike-slip fault (Kyrgyz West Tianshan) as revealed by  $^{40}\text{Ar}/^{39}\text{Ar}$  dating of syn-kinematic white mica. *Journal of Asian Earth Sciences*, 67–68, 76–92.

Roger, F., Jolivet, M., and Malavieille, J. (2010). The tectonic evolution of the Songpan Garzê (North Tibet) and adjacent areas from Proterozoic to Present: a synthesis. *Journal of Asian Earth Sciences*, 39, 254-269.

Rojas-Agramonte, Y., Kröner, A., Alexeiev, D. V., Jeffreys, T., Khudoley, A. K., Wong, J., Geng, H., Shu, L., Semiletkin, S.A., Mikolaichuk, A.V., Kiselev, V. V., Yang, J., Seltmann, R. (2014).

Detrital and igneous zircon ages for supracrustal rocks of the Kyrgyz Tianshan and palaeogeographic implications. *Gondwana Research*, 26(3), 957-974.

Romanovskiy, G. (1880). *Materialien Zur Geologie Von Turkestan. 1. Lieferung. Geologische und Paläontologische Uebersicht Des Nordwestlichen Thian-Schan Und Des Südöstlichen Theiles Des Niederung Von Turan.* Acad. Wissenchaften, St Petersburg, pp 143.

Safonova, I., Biske, G., Romer, R. L., Seltmann, R., Simonov, V., Maruyama, S. (2016). Middle Paleozoic mafic magmatism and ocean plate stratigraphy of the South Tianshan, Kyrgyzstan. *Gondwana Research*, 30, 236-256.

Schnyder, J., Pons, D., Yans, J., Tramoy, R., Abdulanova, S. (2016). Integrated stratigraphy of a continental Pliensbachian-Toarcian Boundary (Lower Jurassic) section at Taskomirsay, Leontiev Graben, southwest Kazakhstan. *In: Brunet, M.-F., McCann, T. Sobel, E.R. (Eds.), Geological Evolution of Central Asian Basins and the Western Tien Shan Range.* Geological Society, London, Special Publications, 427, doi:10.1144/SP427.15

Schoene, B., and Bowring, S. A. (2006) U–Pb systematics of the McClure Mountain syenite: thermochronological constraints on the age of the  $^{40}\text{Ar}/^{39}\text{Ar}$  standard MMhb. *Contributions to Mineralogy and Petrology*, 151, 615–630.

Schwab, M., Ratschbacher, L., Siebel, W., McWilliams, M., Minaev, V., Lutkov, V., Chen, F., Stanek, K., Nelson, B., Frisch, W., Wooden, J. L. (2004). Assembly of the Pamirs: Age and

origin of magmatic belts from the southern Tien Shan to the southern Pamirs and their relation to Tibet. *Tectonics*, 23, TC4002, doi:10.1029/2003TC001583.

Seltmann, R., Konopelko, D., Biske, G., Divaev, F., Sergeev, S. (2011). Hercynian post-collisional magmatism in the context of Paleozoic magmatic evolution of the Tien Shan orogenic belt. *Journal of Asian Earth Sciences*, 42, 821-838.

Sengör, A.M.C. (1984). The Cimmeride Orogenic System and the Tectonics of Eurasia. *Geological Society of America Special papers*, 195, p. 1-74.

Sengör, A.M.C., Natal'in, B.A., Burtman, V.S. (1993). Evolution of the Altaid Tectonic Collage and Paleozoic Crustal Growth in Eurasia. *Nature*, 364 (6435), 299-307.

Shen, P., Shen, Y., Li, X.-H., Pan, H., Zhu, H., Meng, L., Dai, H. (2012). Northwestern Junggar Basin, Xiemisitai Mountains, China: a geochemical and geochronological approach. *Lithos* 140–141, 103–118.

Shen, P., Pan, H., Xiao, W., Chen, X., Seitmuratova, E., Shen, Y. (2013). Two geodynamic–metallogenic events in the Balkhash (Kazakhstan) and the West Junggar (China): Carboniferous porphyry Cu and Permian greisen W–Mo mineralization. *International Geology Review*, 55, 1660–1687.

Shlezinger A. E. (1971). A comparative tectonic analysis of the East Fergana trough and the Greater Karatau graben, *Geotektonika*, 1, 84–95 (in Russian).

Shu, L.S., Deng, X.L., Zhu, W.B., Ma, D.S., Xiao, W.J. (2011). Precambrian tectonic evolution of the Tarim Block, NW China: new geochronological insights from the Quruqtagh domain. *Journal of Asian Earth Sciences* 42, 774–790.

Simonov, V. A., Mikolaichuk, A. V., Rasskazov, S. V., Kovyazin, S. V. (2008). Cretaceous-Paleogene within-plate magmatism in Central Asia: data from the Tien Shan basalts. *Russian Geology and Geophysics*, 49, 520-533.

Simonov, V. A., Mikolaichuk, A. V., Safonova, I. Yu., Kotlyarov, A. V., Kovyazin, S. V. (2015). Late Paleozoic-Cenozoic intra-plate continental basaltic magmatism of the Tianshan-Junggar region in the SW central Asian Orogenic Belt. *Gondwana Research*, 27, 1646-1666.

Sláma, J., Kosler, D., Condon, D.J., Crowley, J.L., Gerdes, A., Hanchar, J.M., Horstwood, M.S.A., Morris, G.A., Nasdala, L., Norberg, N., Schaltegger, U., Schoene, B., Tubrett, M.N., Whitehouse, M.J. (2008). Plesovice zircon — a new natural reference material for U–Pb and Hf isotopic microanalysis. *Chemical Geology*, 249, 1–35.

Sláma, J. and Kosler, J. (2012). Effects of sampling and mineral separation on accuracy of detrital zircon studies. *Geochemistry, Geophysics, Geosystems*, 13, Q05007.

Sobel, E. R., Dumitru, T. A. (1997). Thrusting and exhumation around the margins of the western Tarim Basin during the India-Asia collision. *Journal of geophysical research*, 102, 5043-5063.

Sobel, E. R. (1999). Basin analysis of the Jurassic-Lower Cretaceous southwest Tarim Basin, northwest China. *Geological Society of America Bulletin*, 111 (5), 709-724.

Sobel, E. R., Arnaud, N. (2000). Cretaceous-Paleogene basaltic rocks of the Tuyon Basin, NW China and the Kyrgyz Tian Shan: the trace of a small plume. *Lithos*, 50, 191-215.

Sobel, E. R., Chen, J., Heermance, R. V. (2006a). Late Oligocene – Early Miocene initiation of shortening in the Southwestern Chinese Tian Shan: Implications for Neogene shortening rate variations. *Earth and Planetary Science Letters*, 247, 70-81.

Sobel, E.R., Oskin, M., Burbank, D., Mikolaichuk, A. (2006b). Exhumation of basement-cored uplifts: Example of the Kyrgyz Range quantified with apatite fission track thermochronology. *Tectonics*, 25, TC2008, doi:10.1029/2005TC001809

Stacey, J.S., and Kramers, J.D. (1975). Approximation of terrestrial lead isotope evolution by a two-stage model. *Earth and Planetary Science Letters*, 26, 207–221.

Sun, J., Xiao, W., Windley, B. F., Ji, W., Fu, B., Wang, J., Jin, C. (2016). Provenance change of sediment input in the northeastern foreland of Pamir related to collision of the Indian Plate with the Kohistan-Ladakh arc at around 47 Ma. *Tectonics*, 35, 315-338.

Svendsen, J., Stollhofen, H., Krapf, C. B. E., Stanistreet, I. G. (2003). Mass and hyperconcentrated flow deposits record dune damming and catastrophic breakthrough of ephemeral rivers, Skeleton Coast Erg, Namibia. *Sedimentary Geology*, 160, 7 – 31.

Tang, G.-J., Wang, Q., Wyman, D., Sun, M., Li, Z.-X., Zhao, Z.-H., Sun, W.-D., Jia, X.-H., Jiang, Z.-Q. (2010). Geochronology and geochemistry of Late Paleozoic magmatic rocks in the Lamasu-Dabate area, northwestern Tianshan (west China): Evidence for a tectonic transition from arc to post-collisional setting. *Lithos*, 119, 393-411.

Tang, W., Zhang, Z., Li, J., Li, K., Luo, Z., Chen, Y. (2015). Mesozoic and Cenozoic uplift and exhumation of the Bogda Mountain, NW China: Evidence from apatite fission track analysis. *Geoscience Frontiers*, 6, 617-625.

Tapponnier, P., Molnar, P. (1979). Active faulting and Cenozoic tectonics of the Tien Shan, Mongolia, and Baykal regions. *Journal of Geophysical Research*, 84, 3425–3459.

Teipel, U., Eichhorn, R., Loth, G., Rohrmüller, J., Höll, R., Kennedy, A. (2004). U-Pb SHRIMP and Nd isotopic data from the western Bohemian Massif (Bayerischer Wald, Germany): implications for Upper Vendian and Lower Ordovician magmatism. *International Journal of Earth Sciences*, 93, 782-801.

Thomas, J.C., Cobbold, P.R., Shein, V.S., Le Douaran, S. (1999). Sedimentary record of late Paleozoic to Recent tectonism in Central Asia – analysis of subsurface data from the Turan and Kazak domains. *Tectonophysics*, 313, 243-263.

Tibaldi, A., Corazzato, C., Rust, D., Bonali, F.I., Pasquarè Mariotto, F.A., Korzhenkov, A.M., Oppizzi, P., Bonzanigo, I. (2015). Tectonic and gravity-induced deformation along the active Talas-Fergana Fault, Tien Shan, Kyrgyzstan. *Tectonophysics*, 657, 38-62.

Trifonov, V.G., Korzhenkov, A.M., Omar, K.M. (2015). Recent geodynamics of major strike-slip zones. *Geodesy and Geodynamics*, 6(5), 361-383.

Turdukulov, A. T. (1987). *Geology of the Paleogene and Neogene of North Kyrgyzia*. Ilim Publications, Frunze (Bishkek), Kyrgyzstan, 264 pp. (in Russian).

van Achterbergh, E., Ryan, C. G., Jackson, S. E., Griffin, W. L. (2001). Data reduction software for LA-ICP-MS: appendix. In: *Laser Ablation-ICP-Mass Spectrometry in the Earth Sciences: Principles and Applications*. In Mineralog Assoc Canada (MAC) Short Courses Series (Sylvester, P.J., eds), Ottawa, Ontario, Canada 29,239-243.

Van der Voo, R., Levashova, N.M., Skrinnik, L.I., Kara, T.V., Bazhenov, M.L. (2006). Late orogenic large-scale rotations in the Tien Shan and adjacent mobile belts in Kyrgyzstan and Kazakhstan. *Tectonophysics*, 426, 335-360.

Vermeesch, P. (2012). On the visualisation of detrital age distributions. *Chemical Geology*, 312-313, 190-194.

Vermeesch, P. (2013). Multi-sample comparison of detrital age distributions. *Chemical Geology*, 341, 140-146.

Vermeesch, P., Resentini, A., Garzanti, E. (2016). An R package for statistical provenance analysis. *Sedimentary Geology*, 336, 14-25.

Verzilin, N.N. (1976). A Cretaceous basalt of Fergana and its paleogeographic significance. *Doklady Earth Sciences*, 226, 53–56.

Vialov, O. S. (1948). Paleogenovie Ustrici Tadzhikskoi Depressii (Paleogene Ostreids from Tajik Depression). *Trudy VNIGRI, Leningrad*.

Wack, M. R., Gilder, S. A., Macaulay, E. A., Sobel, E. R., Charreau, J., Mikolaichuk, A. (2014). Cenozoic magnetostratigraphy and magnetic properties of the southern Issyk-Kul Basin, Kyrgyzstan. *Tectonophysics*, 629, 14-26.

Wang, B., Jahn, B-m., Shu, L., Li, K., Chung, S-l., Liu, D. (2012). Middle-Late Ordovician arc-type plutonism in the NW Chinese Tianshan: Implications for the accretion of the Kazakhstan continent in Central Asia. *Journal of Asian Earth Sciences*, 49, 40-53.

Wang, Y., Cai, K., Sun, M., Xiao, W., De Grave, J., Wan, B., Bao, Z. (2017). Tracking the multi-stage exhumation history of the western Chinese Tianshan by Apatite Fission Track (AFT) dating: Implication for the preservation of epithermal deposits in the ancient orogenic belt. *Ore Geology Reviews* (in press). doi:10.1016/j.oregeorev.2017.04.011

Watson, M. P., Hayward, A. B., Parkinson, D. N., Zhang, Zh. M. (1987). Plate tectonic history, basin development and petroleum source rock deposition onshore China. *Marine and Petroleum Geology*, 4 (3), 205-225.

Wilhem, C., Windley, B. F., Stampfli, G. M. (2012). The Altaids of Central Asia: A tectonic and evolutionary innovative review. *Earth-Science Reviews*, 113, 303-341.

Windley, B.F., Alexeiev, D., Xiao, W., Kröner, A., Badarch, G. (2007). Tectonic models for the accretion of the Central Asian Orogenic Belt. *Journal of the Geological Society of London*, 164, 31-47.

Worthington, J. R., Kapp, P., Minaev, V., Chapman, J. B., Mazdab, F. K., Ducea, M. N., Oimahmadov, I., Gadoev, M. (2017). Birth, life, and demise of the Andean – syn-collisional Gissar arc: Late Paleozoic tectono-magmatic-metamorphic evolution of the southwestern Tian Shan, Tajikistan. *Tectonics*, doi: 10.1002/2016TC004285.

Xiao, W., Windley, F., Allen, B., Han, C. (2013). Paleozoic multiple accretionary and collisional tectonics of the Chinese Tianshan orogenic collage. *Gondwana Research*, 23, 1316-1341.

Xiao, W., Santosh, M. (2014). The western Central Asian Orogenic Belt: A window to accretionary orogenesis and continental growth. *Gondwana Research*, 25, 1429-1444.

Xiao, W., Kusky, T., Safonova, I., Seltmann, R., Sun, M. (2015). Tectonics of the Central Asian Orogenic Belt and its Pacific analogues. *Journal of Asian Earth Sciences*, 113 (1), 1-6.

Yang, W., Jolivet, M., Dupont-Nivet, G., Guo, Z., Zhang, Z., Wu, C. (2013). Source to sink relations between the Tian Shan and Junggar Basin (northwest China) from Late Palaeozoic to Quaternary: evidence from detrital U-Pb zircon geochronology. *Basin Research*, 25, 219-240.

Yang, W., Jolivet, M., Dupont-Nivet, G., Guo, Z. (2014). Mesozoic-Cenozoic tectonic evolution of southwestern Tian Shan: Evidence from detrital zircon U/Pb and apatite fission track ages of the Ulugqat area, Northwest China. *Gondwana Research*, 26, 986-1008.

Yang, W., Dupont-Nivet, G., Jolivet, M., Guo, Z., Bougeois, L., Bosboom, R., Zhang, Z., Zhu, B., Heilbronn, G. (2015). Magnetostratigraphic record of the early evolution of the southwestern Tian Shan foreland basin (Ulugqat area), interactions with Pamir indentation and India-Asia collision. *Tectonophysics*, 644-645, 122-137.

Yichun, H., Xuelu, Z., Xianpu, G. (1988). The marine Cretaceous in the western part of the Tarim Basin of Xinjiang: *Acta Geologica Sinica*, 1(1), 13-27.

Yin, A., Harrison, T.M. (2000). Geological evolution of the Himalayan-Tibetan orogen. *Annual review of Earth and Planetary Sciences*, 28, 211-280.

Yin, A. (2010). Cenozoic tectonic evolution of Asia: A preliminary synthesis. *Tectonophysics*, 488, 293-325.

Yin, W., Fan, Z., Zheng, J., Yin, J., Zhang, M., Sheng, X., Guo, J., Li, Q., Lin, Y. (2012). Characteristics of strike-slip inversion structures of the Karatau fault and their petroleum geological significances in the South Turgay Basin, Kazakhstan. *Petroleum Science* 9 (4), 444-454, doi: 10.1007/s12182-012-0228-3.

Zhang, Z., Zhu, W., Zheng, D., Zheng, B., Yang, W. (2016). Apatite fission track thermochronology in the Kuluketage and Aksu areas, NW China: Implication for tectonic evolution of the northern Tarim. *Geoscience Frontiers*, 7, 171-180.

Zorin, Y. A. (1999). Geodynamics of the western part of the Mongolia-Okhotsk collisional belt, Trans-Baikal region (Russia) and Mongolia. *Tectonophysics*, 306, 33-56.

**Figure captions**

Fig. 1. General topographic and tectonic map of Central Asia with indication of the study area. CB= Chu Basin, FB= Fergana Basin, IKB= Issyk-Kul Basin, YFB = Yarkand-Fergana Basin.

Fig. 2: Overview of the study area with indication of the detrital zircon U-Pb sample locations and the study sites. Fergana Basin: Tash-Komyr section (1a), Jetim-Dobo section (1b); Yarkand-Fergana Basin: Terek section (2a), Yassy river (sample KS13-20) (2b), Chitty river (sample KS13-22) (2c); Issyk-Kul Basin: Kadji-Sai section (3a), Jeti-Oguz section (3b); Ming-Kush-Kökömeren Basin: Ming-Kush section (4). NL = Nikolaev Line, TFF = Talas-Fergana Fault, STSs = South Tien Shan suture, MPT = Main Pamir Thrust, NTS = North Tien Shan, MTS = Middle Tien Shan, STS = South Tien Shan, SL = Song-Kul lake, KR = Kapchagay reservoir, KL = Karakul lake. Compilation of zircon U-Pb ages is based on the published database of Käßner et al. (2016) (GSA Data Repository item 2016247) and Macaulay et al. (2016) (Supplementary Table 2, bre12098-sup-0002-Tables2) with addition of extra references of Alexeiev et al. (2016); Bershaw et al. (2012), De Pelsmaeker et al. (2015); Hegner et al. (2010); Konopelko et al. (2013, 2014); Schwab et al. (2004); Simonov et al. (2008).

Fig. 3: Sedimentary logs of the Tash-Komyr and Jetim-Dobo sections in the Fergana Basin. Symbols as in Figure 4. Facies associations and interpretation in terms of depositional environments as in Table 2.

Fig. 4: Sedimentary log of the Terek section in the Yarkand-Fergana Basin. Facies associations and interpretation in terms of depositional environments as in Table 2.

Fig. 5: Sedimentary logs of the Jeti-Oguz, Kadji-Sai and Ming-Kush sections in the Issyk-Kul and Ming-Kush-Kökömeren basins. Symbols as in Figure 4. Facies associations and interpretation in terms of depositional environments as in Table 2.

Fig. 6: Zircon Th/U ratio versus age plot for all detrital samples of this study. Only single-spot ages with 90-110% concordance are plotted. A Th/U ratio of 0.3-0.5 is generally accepted as the lower limit for igneous zircon (Th/U ratios often  $> 0.5$ ), while the upper limit for metamorphic zircon is 0.1 and the values are often lower than 0.01 (Hoskin and Black, 2000; Hoskin and Schaltegger, 2003; Teipel et al., 2004).

Fig 7. Individual sample Kernel density estimation (KDE) diagrams for detrital zircon U-Pb ages from the Tash-Komyr (1a) and Jetim-Dobo (1b) sections in the Fergana Basin; the Terek section (2a), sample KS13-20 (2b), and sample KS13-22 (2c) in the Yarkand-Fergana Basin; and the Kadji-Sai section (3a) in the Issyk-Kul Basin. Open circles below the KDE diagrams represent single-spot ages. Only single-spot ages with 90-110% concordance (amount = n) were used as input in the DensityPlotter program of Vermeesch (2012).

Fig 8: Normalized Kernel density estimation diagrams (Vermeesch et al., 2016) for  $< 541$  Ma detrital zircon U-Pb ages from samples from the Fergana Basin (Tash-Komyr section (1a), Jetim-Dobo section (1b)); the Yarkand-Fergana Basin (Terek section (2a), sample KS13-20 (2b), sample KS13-22 (2c)); and the Issyk-Kul Basin (Kadji-Sai section (3a)). Indication of the depositional age is relative because no accurate depositional age information is available.

TFF = Talas-Fergana Fault.

Fig. 9: Non-metric multidimensional scaling (MDS) diagram of all detrital samples of this study (Vermeesch, 2013; Vermeesch et al., 2016). Less dissimilar samples plot closer together and the closest and second-closest neighbor are indicated with a solid and dashed line respectively.

Fig. 10: Paleogeographic reconstructions of the Kyrgyz Tien Shan during the Jurassic – early Paleogene as described in the text. Boundary of Kyrgyzstan (black solid line) and study sites (yellow dots) as reference position. Fergana Basin: Tash-Komyr section (1a), Jetim-Dobo section (1b); Yarkand-Fergana Basin: Terek section (2a), Yassy river (sample KS13-20) (2b), Chitty river (sample KS13-22) (2c); Issyk-Kul Basin: Kadji-Sai section (3a), Jeti-Oguz section (3b); Ming-Kush-Kökömeren Basin: Ming-Kush section (4). TFF = Talas-Fergana Fault. Grey = erosion prone area; brown = alluvial fan environments; yellow = proximal alluvial plain environments; green = distal alluvial plain environments; light blue = lake; dark blue = sea.

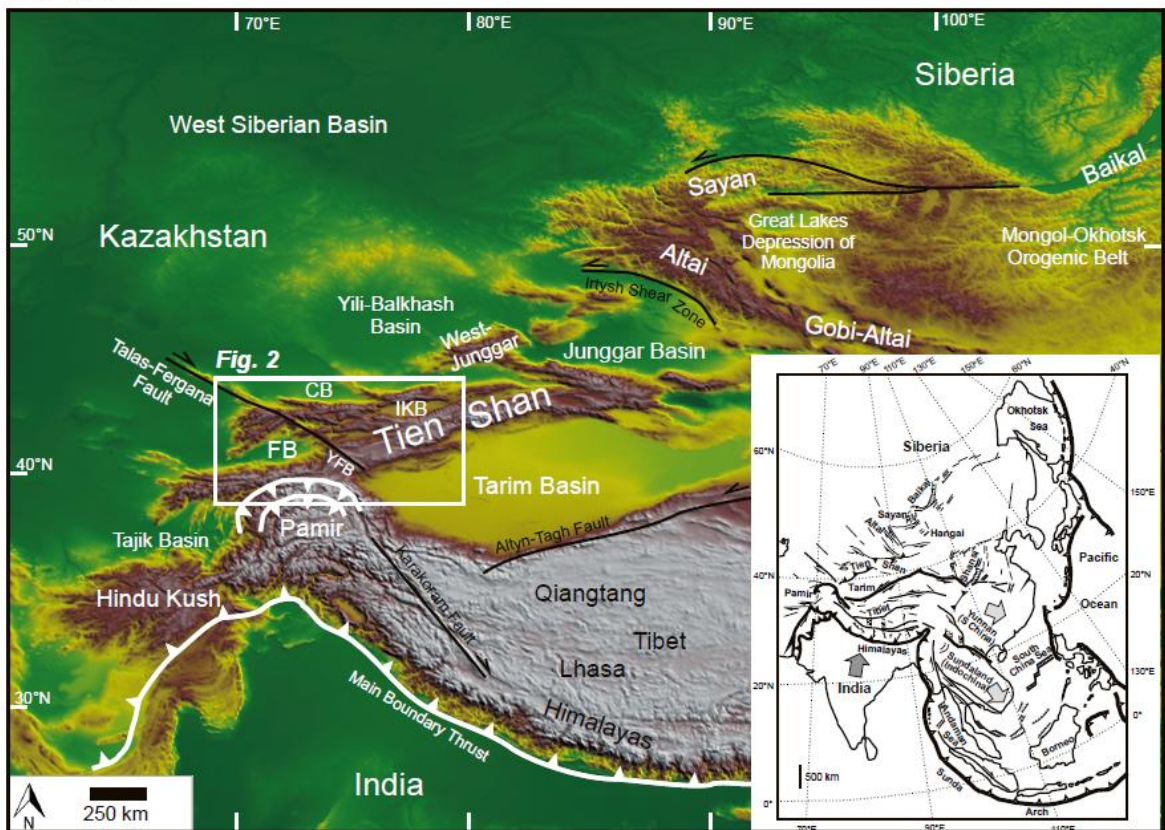
**Table captions**

Table 1: Samples analyzed for detrital zircon U-Pb dating with indication of sample coordinates, lithology, stratigraphic position (J. = Jurassic, Cr. = Cretaceous, Pg. = Paleogene), total number of analyzed grains and number of concordant grains.

Table 2: Facies associations, description of the related sedimentary features and interpretation in terms of depositional environments.

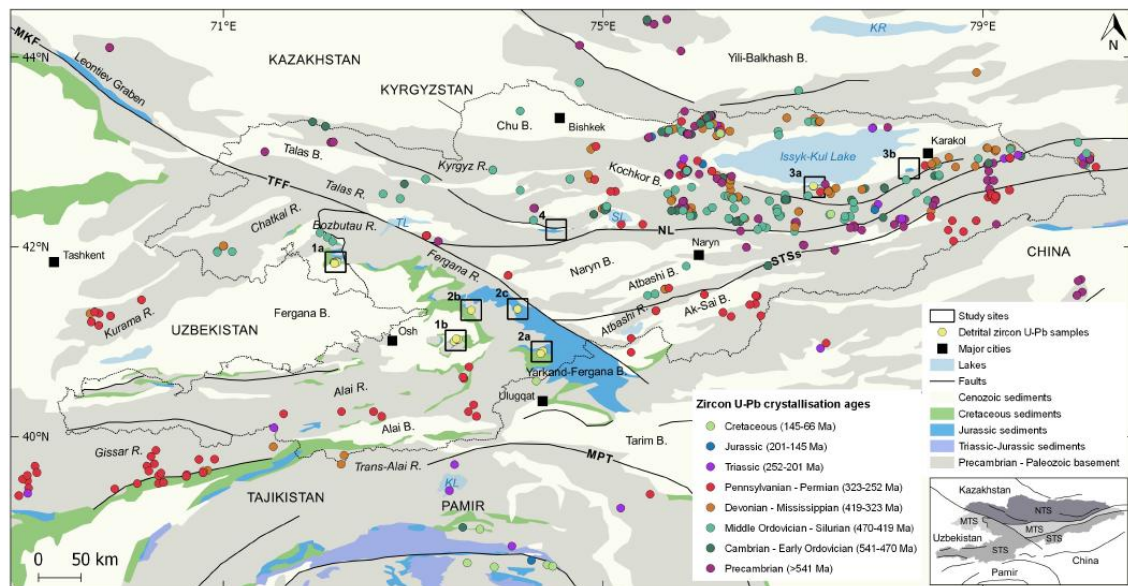
ACCEPTED MANUSCRIPT

Fig. 1 (color)



ACCEPTED

Fig.2



ACCEPTED MANUSCRIPT

Figure 3

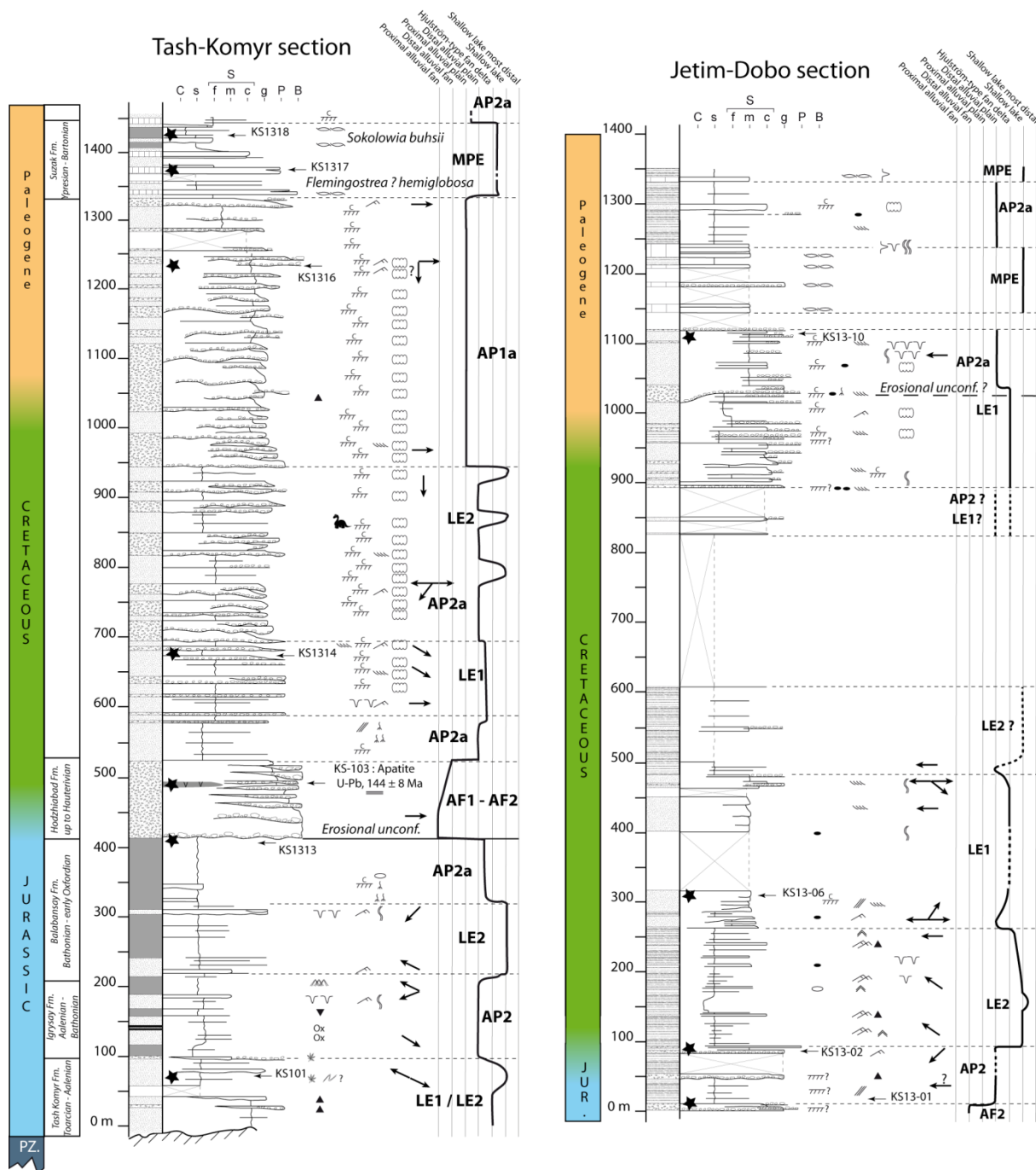
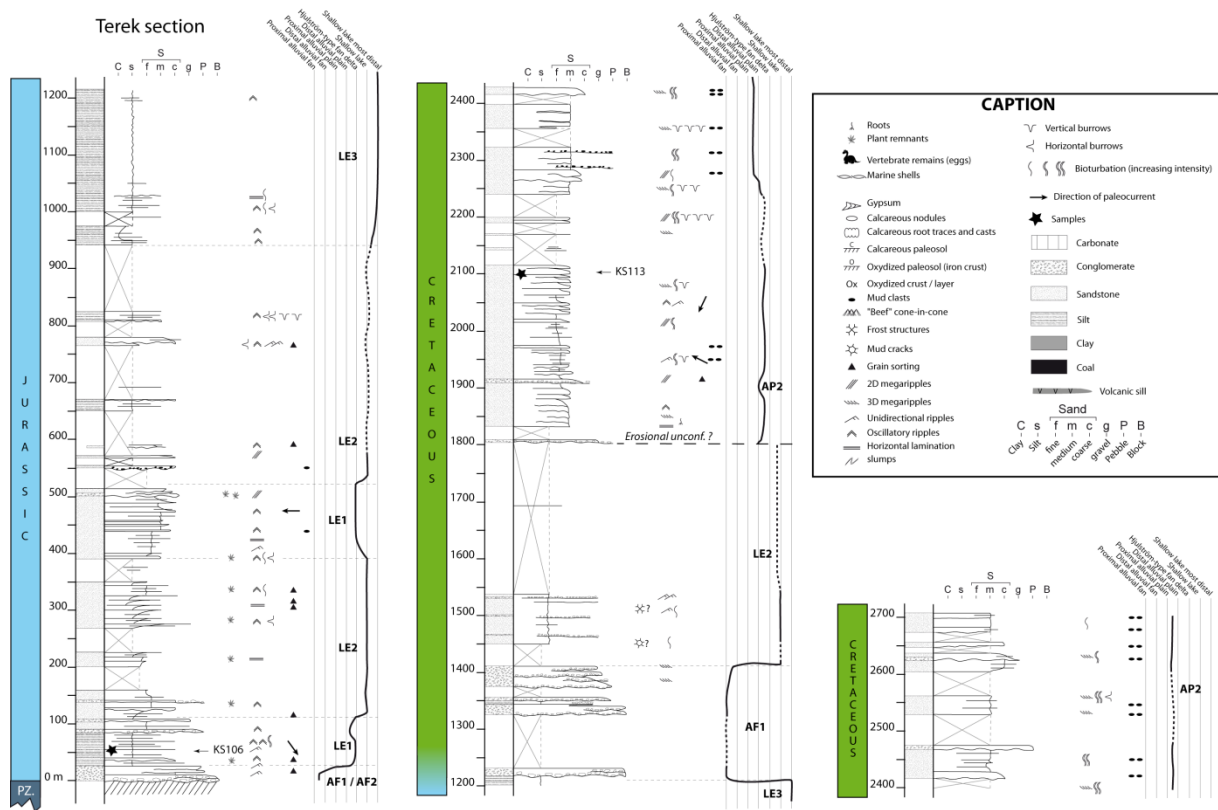


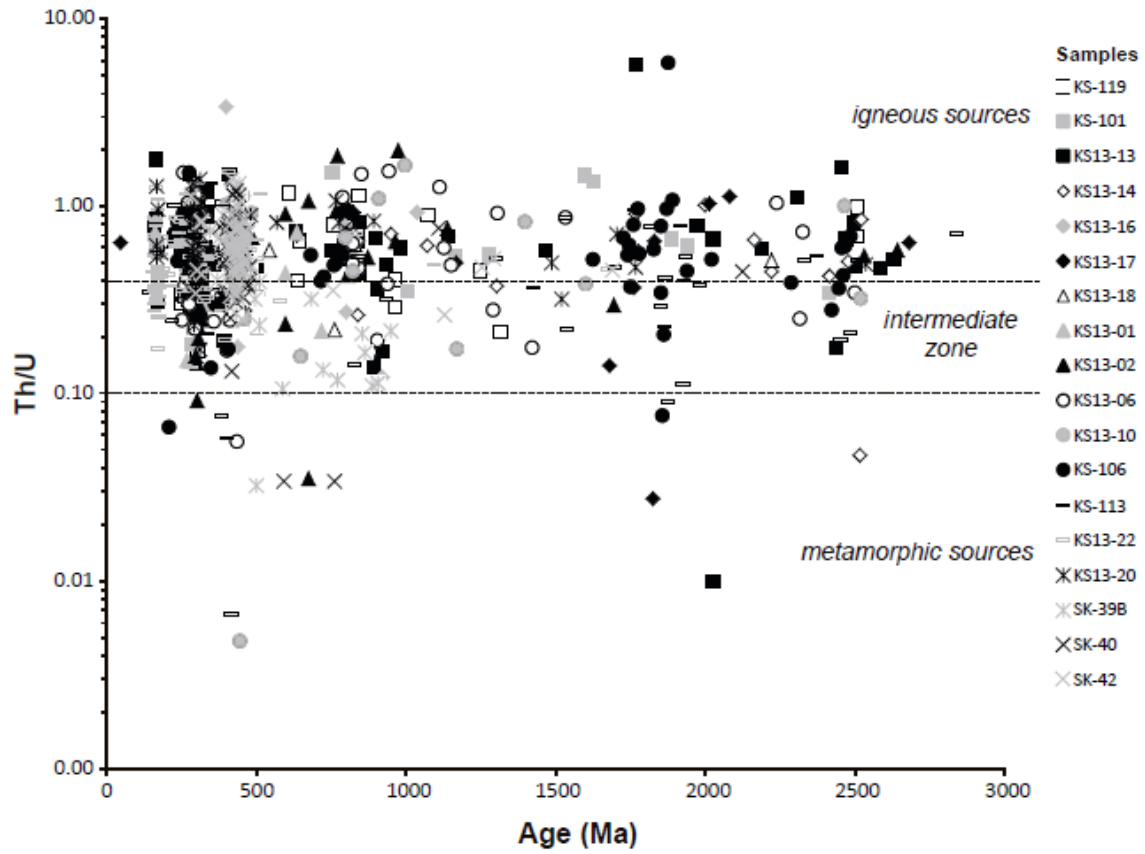
Figure 4



ACCEPTED



Fig. 6



Y

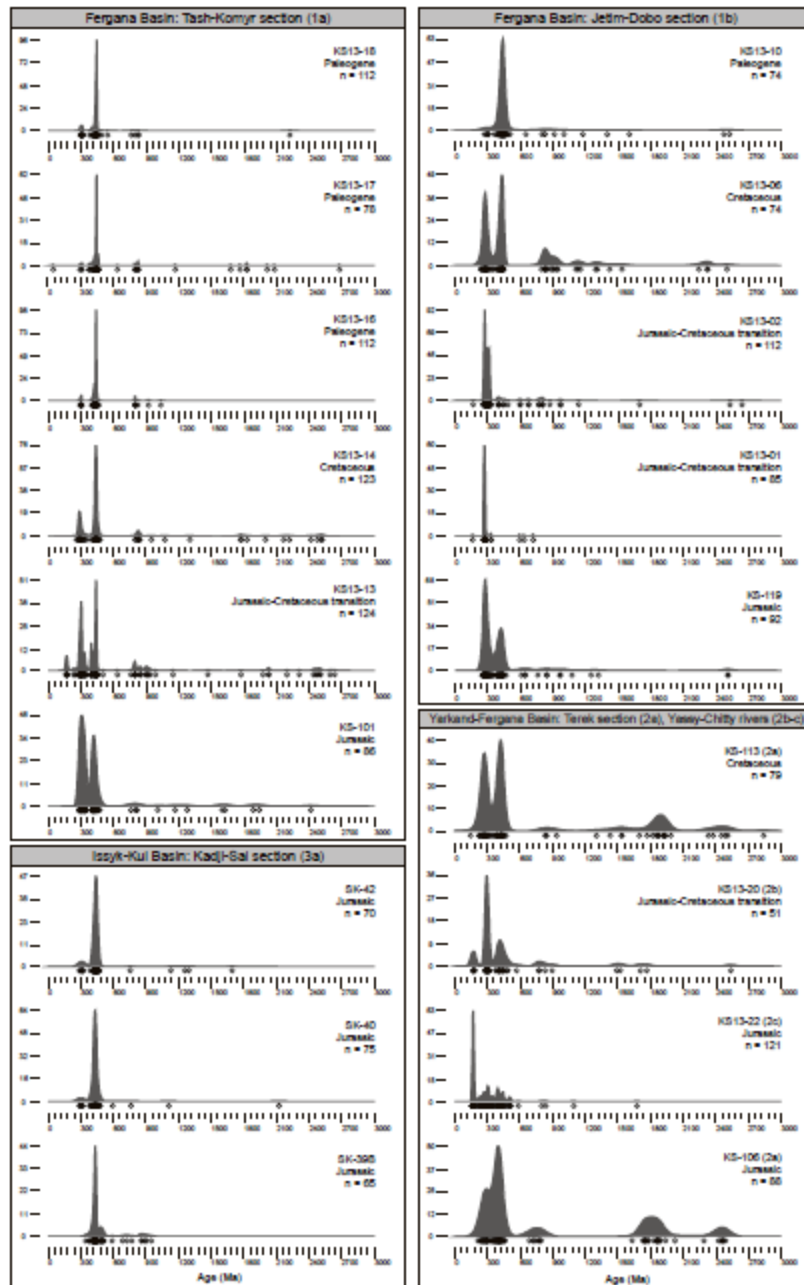
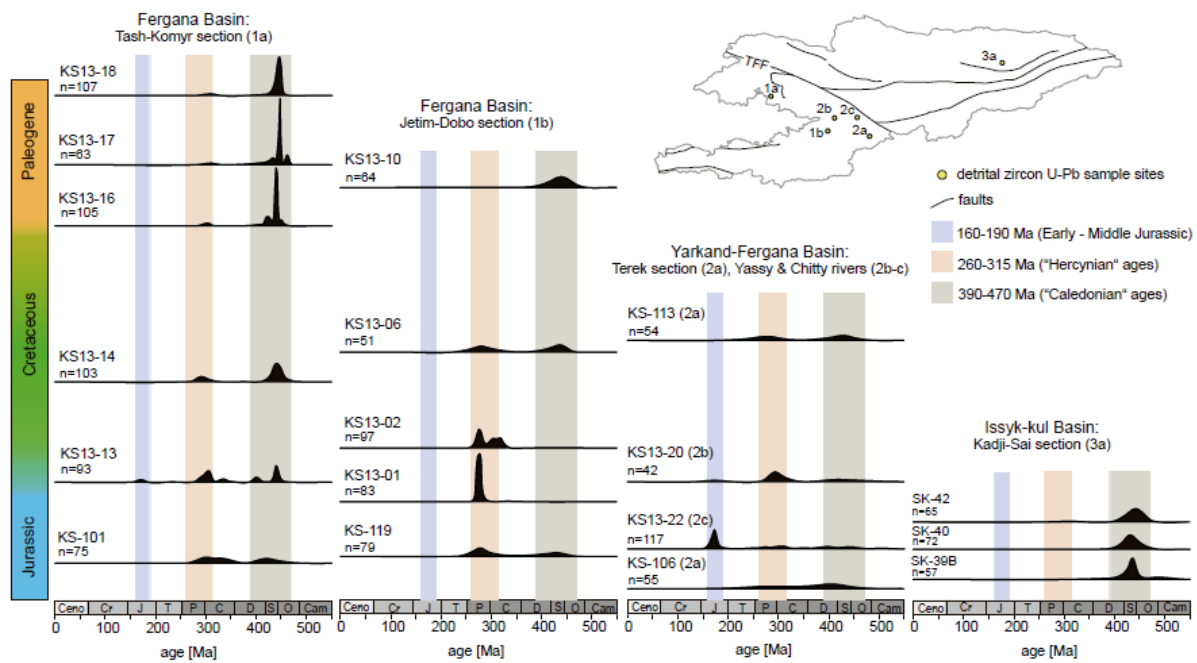


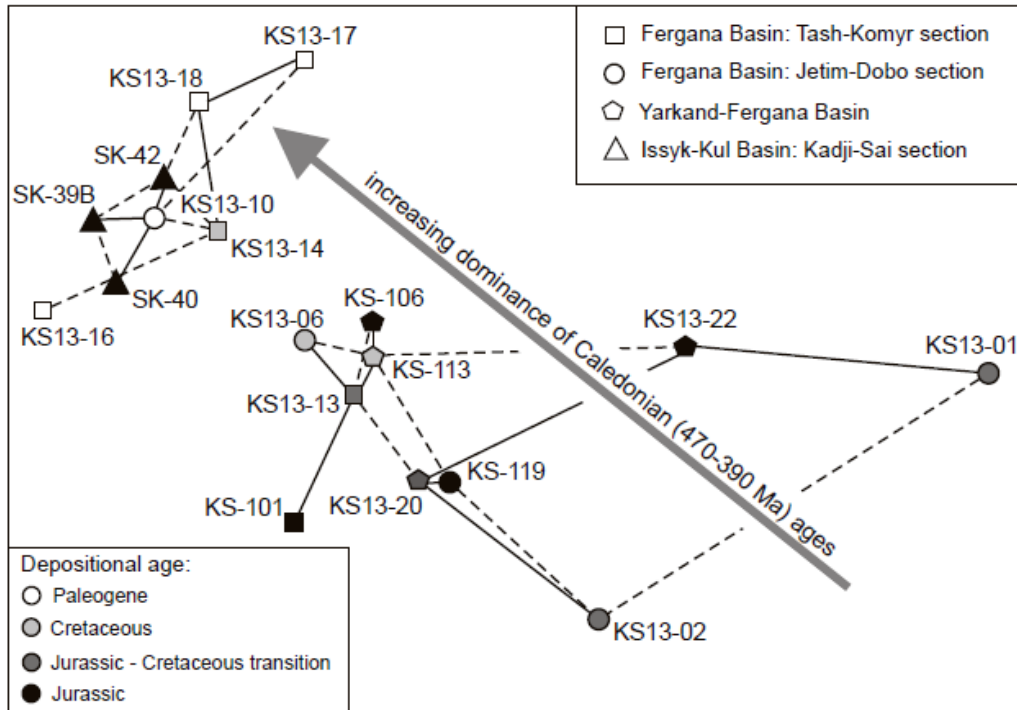
Fig. 7

Fig. 8



ACCEPTED MANUSCRIPT

Fig. 9



ACCEPTTEL

Figure 10

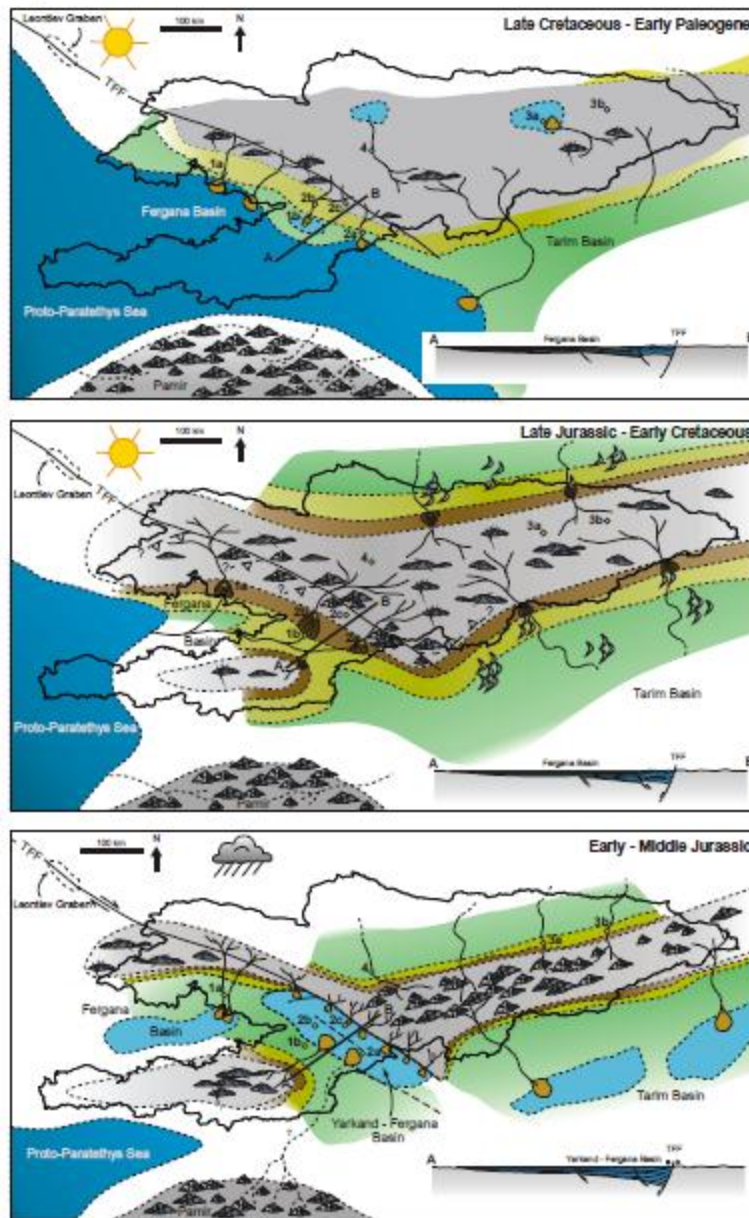


Table1

Sample	Latitude (N)	Longitude (E)	Alt. (m)	Sample site	Lithology	Stratigraphic position	Total no. of grains	No. of conc. grains
KS-101	41°20'4 9.08"	72°11'4 1.00"	686	Fergana Basin (Tash-Komyr)	medium-grained sandstone	J.	88	86
KS13-13	41° 20' 15.19"	72° 9' 41.59"	777	Fergana Basin (Tash-Komyr)	coarse-grained sandstone	J.-Cr. boundary	126	124
KS13-14	41° 20' 5.89"	72° 9' 55.20"	783	Fergana Basin (Tash-Komyr)	medium-grained sandstone	Cr.	125	123
KS13-16	41° 19' 41.11"	72° 10' 10.19"	664	Fergana Basin (Tash-Komyr)	coarse-grained sandstone	Pg.	116	112
KS13-17	41° 19' 35.13"	72° 10' 10.92"	648	Fergana Basin (Tash-Komyr)	coarse-grained sandstone	Pg.	80	78
KS13-18	41° 19' 33.01"	72° 10' 10.94"	636	Fergana Basin (Tash-Komyr)	fine-grained sandstone	Pg.	114	112
KS-119	40° 30' 11.82"	73° 25' 45.56"	211 2	Fergana Basin (Jetim-Dobo)	medium-grained sandstone	J.	96	92
KS13-01	40° 31' 28.46"	73° 27' 57.70"	189 8	Fergana Basin (Jetim-Dobo)	medium-grained sandstone	J.-Cr. boundary	85	85
KS13-02	40° 31' 30.72"	73° 27' 56.92"	190 5	Fergana Basin (Jetim-Dobo)	fine-grained sandstone	J.-Cr. boundary	114	112
KS13-06	40° 31' 40.07"	73° 28' 21.25"	193 3	Fergana Basin (Jetim-Dobo)	medium-grained sandstone	Cr.	82	74
KS13-10	40° 31' 56.43"	73° 27' 0.59"	232 8	Fergana Basin (Jetim-Dobo)	medium-grained sandstone	Pg.	82	74
KS-106	40° 24' 0.78"	74° 21' 53.58"	299 2	Yarkand-Fergana Basin (Terek)	medium-grained sandstone	J.	95	88
KS-113	40° 22' 34.14"	74° 20' 28.86"	265 1	Yarkand-Fergana Basin (Terek)	medium-grained sandstone	Cr.	83	79
KS13-20	40° 50' 0.46"	73° 36' 35.59"	137 0	Yarkand-Fergana Basin (Yassy river)	medium-grained sandstone	J.-Cr. boundary	67	51
KS13-22	40° 50' 42.27"	74° 5' 59.61"	250 1	Yarkand-Fergana Basin (Chitty river)	fine-grained sandstone	J.	122	121
SK-39B	42° 08' 22.62"	77° 12' 56.58"	192 6	Issyk-Kul Basin (Kadji-Sai)	coarse-grained sandstone	J.	78	65
SK-40	42° 08' 22.50"	77° 12' 54.42"	191 6	Issyk-Kul Basin (Kadji-Sai)	fine-grained sandstone	J.	78	75
SK-42	42° 08' 34.98"	77° 12' 55.92"	184 1	Issyk-Kul Basin (Kadji-Sai)	medium-grained sandstone	J.	83	70

Table 1: Samples analyzed for detrital zircon U-Pb dating with indication of sample coordinates, lithology, stratigraphic position (J. = Jurassic, Cr. = Cretaceous, Pg. = Paleogene), total number of analyzed grains and number of concordant grains.

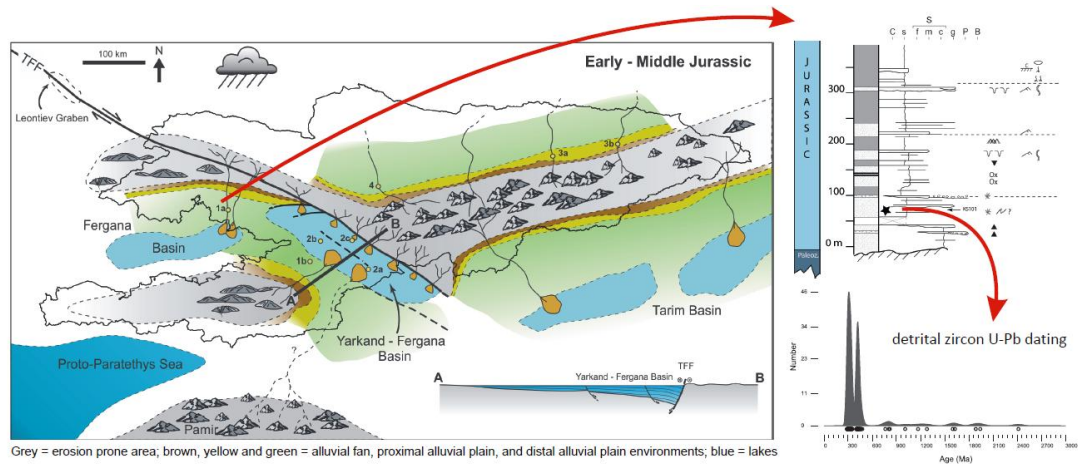
Facies associations	Sedimentary features	Depositional environments
AF1	Alternation of poorly stratified pluri-decimeter- to pluri-meter-thick mainly structure-less gravel to boulder conglomerates and of centimeter- to decimeter-thick coarse-grain to gravel sandstones generally in lenses. Clast-supported conglomerates characterized by erosive bases and angular to sub-angular, poorly sorted clasts. Current ripples in finer-grained lenses.	Proximal alluvial fan (e.g. Blair and McPherson, 1994; Blair, 1999; Mulder and Alexander, 2001; Svendsen et al., 2003)
AF2	Alternation of decimeter- to meter-thick planar layers of dominantly poorly sorted, sub-angular pebble conglomerates and of pluri-decimeter- to meter-thick poorly- to well-sorted sandstones with horizontal laminations. Sometimes decimeter- to meter-thick channelled poorly-sorted bed-load deposits with 3D megaripples and floating pebbles. Very rare paleosols (Retallack, 1997). Plant fragments.	Distal alluvial fan (e.g. Blair and McPherson, 1994)
AF2a	Similar to AF2 but containing rare calcareous paleosol layers (calcretes) indicating a semi-arid climate (e.g. Birkeland, 1974; Mack et al., 1993)	Semi-arid distal alluvial fan (e.g. Mather and Hartley, 2005)
AP1	Meter- to several-meters-thick stacked, strongly erosive, channelized, coarse-grained sandstone to pebbles (including soft pebbles) layers with rare blocks. Current ripples including 3D megaripples. Root traces, oxidized paleosol layers and plant fragments (Retallack, 1997).	Proximal alluvial plain (e.g. Miall, 1996)
AP1a	Similar to AF1 but containing strong pedogenesis marked by frequent several-decimeters to several-meters-thick calcretes and caliches indicating a semi-arid climate (e.g. Mack et al., 1993; Miall, 1996).	Semi-arid proximal alluvial plain (e.g. Miall, 1996)
AP2	Alternation of meter-thick, channelized, medium- to coarse-grained quartz-rich sandstones to well-rounded pebble conglomerates with pluri-decimeters-to pluri-meters-thick siltstones or fine- to very-fine-grained sandstones. Coal layers. The coarser-grained layers show grading, current ripples and mud flakes or coal chips. Plant fragments. Numerous iron-crust layers indicating humid paleosols.	Distal alluvial plain to lacustrine coastal plain (e.g. Miall, 1996)
AP2a	Similar to AP2 but containing strong pedogenesis marked by frequent several-decimeters to several-meters-thick calcretes and caliches indicating a semi-arid climate. The most distal facies are formed by massive siltstones with root traces, calcareous paleosols and calcareous nodules (Hasiotis et al., 2007).	Semi-arid distal alluvial plain to lacustrine coastal plain (e.g. Miall, 1996)
LE1	Meters- to several-meters thick fine-grained sandstones with siltstones, sometimes in lenses, showing rare wave ripples, interbedded with meter-thick coarse-grained sandstone to pebbles layers (sometimes in lenses with erosive base) showing current ripples and grading. Vertical bioturbation. Decimeters- to several-decimeters thick paleosols (caliches or oxidized crusts) indicating emersion (Mack et al., 1993).	Hjulström-type fan delta (e.g. Hjulström, 1952 ; McPherson et al., 1987 ; Postma, 1990)
LE2	Meter- to several-meters-thick siltstones to fine-grained sandstones, with bioturbations (horizontal and/or vertical burrows), interbedded with centimeter- to several-decimeter-thick fine to coarse sandstones with current and rare wave ripples and grading interpreted as high-density gravity flows (Lowe, 1982; Mulder and Alexander, 2001). Plant remains. Rare paleosols with vertical roots, sometimes oxidized or associated to calcareous nodules (Hasiotis et al., 2007).	Shallow lake (e.g. Miall, 2016)
LE3	Massive horizontally laminated siltstones with few centimeter thick layers of fine- to medium-grained sandstones. Wave ripples and bioturbation.	Shallow lake most distal (e.g. Miall, 2016)

MPE	Meter-thick marls containing bivalves, interlayered with decimeter- to meter-thick bioclastic to coquina (mainly formed by oysters) carbonates including some pluri-decimeters- to meter-thick carbonate-cement pebble conglomerates.	Marine protected embayment, subtidal to intertidal (e.g. Lan, 1997; Bosboom et al., 2011)
-----	---	---

Table 2 : Facies associations, description of the related sedimentary features and interpretation in terms of depositional environments.

ACCEPTED MANUSCRIPT

## Graphical Abstract



ACCEPTED MANUSCRIPT